

The 3D Structure of Northern Hemisphere Blocking Events: Climatology, Role of Moisture, and Response to Climate Change[✉]

EBRAHIM NABIZADEH,^a SANDRO W. LUBIS,^a AND PEDRAM HASSANZADEH^a

^a *Rice University, Houston, Texas*

(Manuscript received 15 February 2021, in final form 5 August 2021)

ABSTRACT: To better understand the dynamics and impacts of blocking events, their 3D structure needs to be further investigated. We present a comprehensive composite analysis of the 3D structure of blocks and its response to future climate change over the North Pacific, the North Atlantic, and Russia in summers and winters using reanalysis and two large-ensemble datasets from CESM1 and GFDL-CM3. In reanalysis, over both ocean and land, the anomalous winds are equivalent-barotropic in the troposphere and stratosphere, and temperature anomalies are positive throughout the troposphere and negative in the lower stratosphere. The main seasonal and regional differences are that blocks are larger and/or stronger in winters; over oceans, the temperature anomaly is shifted westward due to latent heating. Analyzing the temperature tendency equation shows that in all three sectors, adiabatic warming due to subsidence is the main driver of the positive temperature anomaly; however, depending on season and region, meridional thermal advection and latent heating might have leading-order contributions too. Both GCMs are found to reproduce the climatological 3D structure remarkably well, but sometimes disagree on future changes. Overall, the future summertime response is weakening of all fields (except for specific humidity), although the impact on near-surface temperature is not necessarily weakened; for example, the blocking-driven near-surface warming over Russia intensifies. The wintertime response is strengthening of all fields, except for temperature in some cases. Responses of geopotential height and temperature are shifted westward in winters, most likely due to latent heating. Results highlight the importance of process-level analyses of blocks' 3D structure for improved understanding of the resulting temperature extremes and their future changes.

KEYWORDS: Atmospheric circulation; Blocking; Extreme events; Climate change; General circulation models

1. Introduction

Blocking events are anomalous large-scale, quasi-stationary, high pressure (anticyclonic) systems that last beyond the synoptic time scales (sometimes for weeks) and block or divert the midlatitude westerlies (Rex 1950; Green 1977; Hoskins and James 2014; Woollings et al. 2018). Due to their persistence and size, depending on the season and the region, blocking events can cause, or contribute to, various types of extreme events such as heat waves, cold spells, droughts, and heavy rainfall episodes (e.g., Barriopedro et al. 2011; Dole et al. 2011; Pfahl and Wernli 2012; Brunner et al. 2017, 2018; Schaller et al. 2018; Zschenderlein et al. 2019; R othlisberger and Martius 2019; Wehrli et al. 2019; Lenggenhager et al. 2019; Chan et al. 2019). Despite much effort, the dynamical mechanisms responsible for the generation and maintenance of the blocking events are still not well understood (Hoskins and James 2014; Hassanzadeh and Kuang 2015; Schubert and Lucarini 2016; Nakamura and Huang 2018; Woollings et al. 2018; Lucarini and Gritsun 2020). For example, while past studies have often considered blocking dynamics to be dominantly governed by dry processes, most notably through eddy-blocking feedbacks (e.g., Shutts 1983; Illari and Marshall 1983; Nakamura et al. 1997; Cash and Lee 2000; Yamazaki and Itoh 2013; Luo et al.

2019), a few recent studies have used Lagrangian trajectory tracking and shown a leading-order contribution from latent heating to blocking dynamics in some cases (Pfahl et al. 2015; Steinfeld and Pfahl 2019; Steinfeld et al. 2020).

There has been extensive research in the past two decades on how blocking events might change as the climate warms (Woollings et al. 2018). Most studies have focused on effects of climate change on the frequency of the blocking events and the corresponding weather extremes (e.g., Wiedenmann et al. 2002; Barnes et al. 2014; Hassanzadeh et al. 2014; Barnes and Polvani 2015; Horton et al. 2015; Kennedy et al. 2016; Peings et al. 2017; Coumou et al. 2018; Patterson et al. 2019; Narinesingh et al. 2020; Davini and D'Andrea 2020; Lackmann et al. 2021), while a few studies have investigated the effects on the average duration of blocking events (Barnes et al. 2012; Huguenin et al. 2020; Narinesingh et al. 2020; Lackmann et al. 2021) or their size (i.e., spatial extent; Nabizadeh et al. 2019).

Another aspect of blocking events that needs to be studied to better understand their dynamics and impacts (e.g., on surface weather) is their three-dimensional (3D) structure. Blocking events are often identified and examined on a single level (mainly at 500 hPa) with their signature in the surface temperature sometimes considered as well. That said, there are a few exceptions, such as the indices that identify blocking events on higher levels (e.g., Hoskins et al. 1985; Brunner et al. 2016) or the index introduced by Schierz et al. (2004), which identifies blocks based on the integrated potential vorticity (PV) between 500 and 150 hPa. A few case studies analyzed blocking events on more than one level and found equivalent-barotropic structures throughout the troposphere (Green 1977; Tsou and Smith 1990; Mak 1991; Lupo and Smith 1995; Ma and Liang 2017).

[✉] Supplemental information related to this paper is available at the Journals Online website: <https://doi.org/10.1175/JCLI-D-21-0141.s1>.

Corresponding author: Pedram Hassanzadeh, pedram@rice.edu

Using several reanalysis datasets and one decade of global positioning system (GPS) radio occultation data, [Brunner and Steiner \(2017\)](#) studied, among other things, the vertical structure of composited temperature (T) and specific humidity (SP) of winter and summer blocking events over three ocean basins: the North Atlantic, North Pacific, and eastern Pacific (Southern Hemisphere). They found relatively height-independent anomalous positive T structures in the troposphere, with a reversal to negative anomaly above the tropopause, which was also reported by [Green \(1977\)](#) in his case study. [Brunner and Steiner \(2017\)](#) found a more complex 3D structure for SP (discussed later).

Motivated by understanding the dynamics of blocking-driven heat waves and their future changes, some studies have investigated the physics of the positive temperature anomaly throughout the troposphere and/or near the surface (e.g., [Bieli et al. 2015](#); [Kennedy et al. 2016](#); [Wehrli et al. 2019](#); [Zschenderlein et al. 2019, 2020](#)). For example, [Zschenderlein et al. \(2019\)](#) used Lagrangian trajectory analysis and Eulerian calculations of horizontal temperature advection to quantify the role of different physical processes in European heat waves. They found that temperature increases adiabatically due to the subsidence of air throughout the troposphere with negligible contribution from horizontal thermal advection, and that diabatic heating intensifies the amplitude of this increase just near the surface, where vertical advection is negligible.

Building on the aforementioned studies and motivated by questions about the dynamics and impacts of blocking events in a changing climate, in this paper we present a comprehensive analysis of the climatology of the 3D structure of blocking events and its response to climate change in summer and winter in Northern Hampshire (NH) over two ocean basins (North Atlantic and North Pacific) and one land sector (Russia). Using the composite analysis of the 3D velocity (u, v, ω), geopotential height (Z), T , and SP fields in data from ERA-Interim, two sets of large-ensemble comprehensive GCM simulations, and idealized dry and moist GCMs, we aim to address the following specific questions:

- 1) What does the climatological 3D structure of NH blocking events look like in reanalysis? Are there differences between the structures of blocking events in summer versus winter, and over land versus ocean?
- 2) What is the physics of the temperature anomaly under the blocking anticyclone? What are the relative roles of adiabatic processes (horizontal and vertical thermal advection) and latent heating?
- 3) Do comprehensive GCMs faithfully reproduce the climatological 3D structure of NH blocking events?
- 4) How will the 3D structure of blocking events change in the future under the RCP8.5 radiative forcing scenario?

The remainder of this paper is structured as follows. In [section 2](#), models, data, and methods are presented. The climatological 3D structure of blocking events and the physics of the temperature anomaly in reanalysis (questions 1 and 2) and the 3D structure of blocking events in GCMs (question 3) are discussed in [section 3](#). Response of the blocking events' 3D structure to climate change (question 4) is analyzed in

[section 4](#). The paper ends with a summary of the findings and discussions in [section 5](#).

2. Models, data, and methods

a. Reanalysis data

We use the 6-hourly u, v, ω, Z, T , and SP on various levels from 1979 to 2019 from the ERA-Interim dataset ([Dee et al. 2011](#)). This dataset has a resolution of $0.75^\circ \times 0.75^\circ$. For each variable, daily anomalies are calculated by removing the climatological mean, defined as the 31-day running mean centered around that calendar date and averaged over all 40 years of ERA-Interim data ([Chan et al. 2019](#); [Nabizadeh et al. 2019](#)).

b. Large-ensemble comprehensive GCM simulations

We use daily data from NCAR's CESM1 Large-Ensemble Project (LENS; [Kay et al. 2015](#)) and the GFDL CM3 large-ensemble project (GFDL-LE; [Donner et al. 2011](#); [Sun et al. 2018](#)). These two datasets consist of data from fully coupled GCM simulations at the horizontal resolution of $\sim 1^\circ$ (LENS) and $\sim 2.5^\circ$ (GFDL-LE). The LENS and GFDL-LE ensembles have, respectively, 40 and 20 members for the "current climate" (1920–2005) based on the historical radiative forcing, and the same number of members for the "future climate" (2006–2100) based on the RCP8.5 radiative forcing scenario. The large number of ensemble members and the availability of daily variables in these two datasets are helpful in obtaining a high signal-to-noise ratio for climate change response of blocking events, which are infrequent ([Schaller et al. 2018](#); [Brunner et al. 2018](#); [Nabizadeh et al. 2019](#)).

We use the last 25 years of each period to investigate the effects of climate change on the 3D structure of blocking events. From each dataset, we use the same variables as in [section 2a](#) on three levels (850, 500, and 200 hPa), except for ω , which was not provided in either dataset and SP, that was not provided in GFDL-LE. From LENS, we also use the 2-m air temperature (T_{2m}). For each variable in each time period, daily anomalies are calculated by removing the climatological mean, defined as the 31-day running mean centered around that calendar date and averaged over all years and ensemble members ([Nabizadeh et al. 2019](#)).

c. Idealized dry and moist GCMs

Two idealized GCMs are used to investigate the role of latent heating on the structure of blocking events. One is the GFDL spectral dry dynamical core GCM with the physics configuration of [Held and Suarez \(1994\)](#). The setup is identical to that of [Hassanzadeh and Kuang \(2016, 2019\)](#), in which the model has flat lower boundaries and is forced by Newtonian relaxation of temperature to a prescribed equinoctial radiative-equilibrium state. The second model is an idealized moist GCM [model of an idealized moist atmosphere (MiMA)], which has a uniform slab ocean with a mixed-layer depth of 7.5 m, seasonal cycle, and a full radiative transfer scheme ([Jucker and Gerber 2017](#); [Garfinkel et al. 2020](#)). Both models are run with a T63 spectral resolution with 40 vertical levels for 100 000 days, with the first 500 days in the dry GCM and first 5 years in MiMA

discarded as spinup. Anomalies in the dry GCM are computed by removing the long-term mean whereas in MiMA the anomalies are computed by removing the climatological mean, defined as the 31-day running mean centered around that date and averaged over all years (Nabizadeh et al. 2019).

d. Blocking index

In ERA-Interim and all GCMs (except for the dry GCM, which is at equinox), we identify and analyze the blocking events separately in summers [June–August (JJA)] and winters [December–February (DJF)]. Furthermore, in ERA-Interim and comprehensive GCMs, we identify and analyze the blocking events separately over three sectors of the NH between 40° and 60°N: North Atlantic (60°W–30°E), North Pacific (125°E–130°W), and Russia (31.25°E–123.75°E). Note that these three sectors are the main regions of blocking activity in the NH (e.g., Dole and Gordon 1983; Woollings et al. 2018). The climatology of the blocking frequency over these regions in reanalysis datasets and climate models has been comprehensively investigated in previous studies (e.g., Barriopedro et al. 2006; Dunn-Sigouin and Son 2013; Small et al. 2013; Barnes et al. 2014; Woollings et al. 2018; Simpson et al. 2020; Wazneh et al. 2021). Furthermore, the response of blocking frequency under climate change in these regions has been well explored in LENS (e.g., Peings et al. 2017; Kwon et al. 2018) and in models from phase 5 of the Coupled Model Intercomparison Project (CMIP5) (Masato et al. 2013; Barnes and Polvani 2015; Cattiaux et al. 2016; Brunner et al. 2018).

To identify the blocking events, we employ the index of Dole and Gordon (1983), which is based on finding strong, stationary, and persistent positive daily geopotential height at 500 hPa (Z500) anomalies (to be quantified below). In a recent study by Chan et al. (2019), this index was found to perform better in identifying the heat wave–causing weather patterns compared to a few other Z500-based indices. In this index, the Z500 anomalies are first scaled by the sine of latitude following Dole and Gordon (1983) and then their standard deviation at each grid point is computed. The maximum standard deviation over latitudes 40°–60°N is used to normalize the Z500 anomalies. It should be highlighted that the standard deviations used for normalizing the anomalies are calculated separately for each sector, season, time period, and GCM/dataset. In this index, any fixed grid points with normalized anomalies larger than 1.5 and persisting for at least 5 consecutive days are identified as blocking episodes [for more details, see Nabizadeh et al. (2019)]. Note that any two blocking episodes that are separated by only one nonblocked day are counted as one blocking event. Moreover, we ignore any blocking events shorter than 5 days in the period of 1 December–28 February or 1 June–31 August.

e. Composite analysis

For each blocking event, we use the average of the first 5 days of their lifetime as their representative. This is the blocking events' mature phase, which is the most relevant phase to the resulting weather extremes. Following Nabizadeh et al. (2019), we identify the center of each block by finding the centroid of the 5-day averaged normalized Z500 anomaly

inside the closed contour line of one standard deviation around the blocked grid point (Nabizadeh et al. 2019). Then all these centers are shifted to one position (in latitude and longitude, referred to herein as the “center” of blocks) and the anomalies of each variable of interest (v , T , etc.) are composited. The number of snapshots that are averaged for composite analysis is in the order of 500, 20 000, and 10 000 for ERA-Interim, LENS, and GFDL-LE, respectively.

3. The 3D structure of blocking events: Climatology

In this section, given our focus on three sectors, two seasons, and several variables, we will often only show the results of one or two representative sector(s) in the paper and highlight and discuss the similarities or differences among all seasons/sectors. Results for the rest of the sectors are presented in the online supplemental material.

a. ERA-Interim: 1979–2019

Figure 1 shows the composites of Z and v anomalies for the wintertime and summertime North Pacific blocking events. Figures S1 and S2 in the supplemental material show similar plots but for blocks in the North Atlantic and Russian sectors, respectively. Consistent among the three sectors and two seasons, blocking events have an equivalent-barotropic anticyclonic pattern throughout the troposphere and lower stratosphere with strong positive Z500 anomalies and a dipolar structure in the v anomalies during winter and summer. One noticeable difference is that wintertime blocks are larger and stronger than the summertime blocks, consistent with previous findings (Brunner and Steiner 2017; Lupo et al. 2019; Nabizadeh et al. 2019; Hwang et al. 2020).

Next, we will first describe some of the main features of the 3D structure of the T , ω , and SP anomalies during blocking events, and will then analyze the adiabatic and diabatic processes in the temperature tendency equation to explain some of these features and the relative importance of these processes.

Figures 2 and 3 show the composites of T , ω , and SP anomalies for the North Pacific blocks in winters and summers, respectively. Figures S3–S6 show similar plots but over the North Atlantic and Russian sectors. Again, consistent among sectors and seasons, temperature has a warm anomaly throughout the troposphere under the anticyclone and then a cold anomaly in the lower stratosphere, consistent with previous findings of Green (1977) and Brunner and Steiner (2017). In winters, there is a cold temperature anomaly to the east and/or southeast side of the blocking center at 500 and 850 hPa. Furthermore, in the winters of North Pacific and North Atlantic (Figs. 2d,h; see also Figs. S3d,h), there is a noticeable westward shift of the temperature anomaly in the troposphere with respect to the blocking center, which was also reported by Brunner and Steiner (2017). We will come back to explaining the underlying mechanism of this shift shortly.

The anomalous vertical velocity (ω) has a maximum around 500 hPa (Figs. 2e and 3e; see also Figs. S3–S6), and while its structure always consists of a descending branch (subsidence) around or to the east of the blocking center, in some cases—such as the North Pacific (both seasons), the North

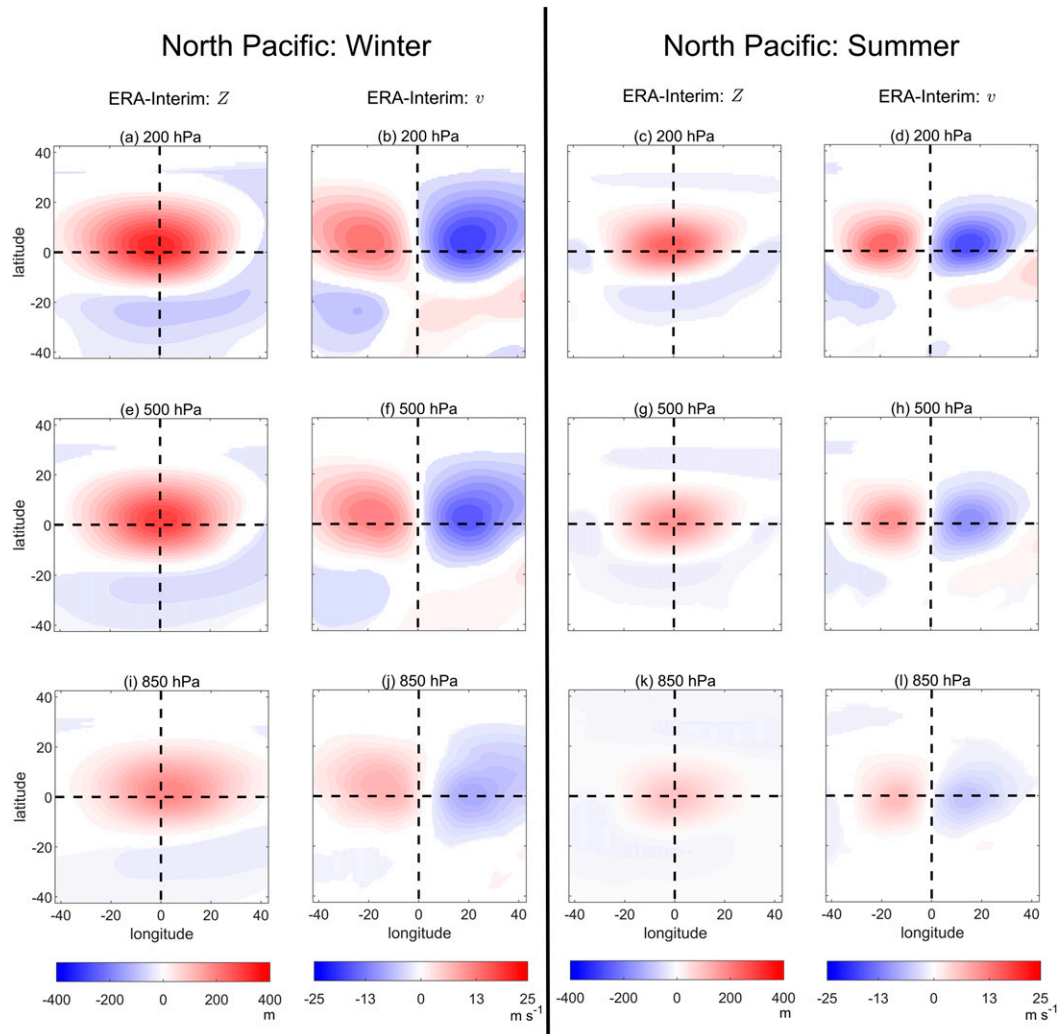


FIG. 1. Composites of anomalous geopotential height (Z) and meridional wind (v) of blocking events in the ERA-Interim (1979–2019) over the North Pacific sector. Rows show (top) 200-, (middle) 500-, and (bottom) 850-hPa levels. The columns are for (left) winter (DJF) blocks and (right) summer (JJA) blocks. In all panels, anomalies are first centered and then composited. The intersection of the dashed lines shows the center, and the latitudes and longitudes are relative to the center. All shown anomalies are significant at 95% level based on a one-sample t test.

Atlantic (winter), and Russia (summer)—its structure also consists of an equally strong ascending branch to the west in the midtroposphere. Mak (1991) reported a similar dipolar structure in ω of a 3-week-long wintertime North Atlantic blocking event. The ascending flow on the western flank of blocking events was also shown in the results of Steinfeld et al. (2020) where they used backward air-parcel trajectories and showed correlations between the ascent on the western flank to the region of intense latent heat release. Mak (1991) also highlighted a broad region of ascending flow on the southeast side of the blocking event in their case study, which is consistent with the results of our composite analysis in the winter of both ocean basins (Fig. 2e; see also Fig. S3e).

The anomalous SP field also has some degree of seasonal and regional dependencies. The maximum of SP anomaly occurs around 850 hPa [panel (j) of Figs 2, 3, and S3–S6]. In all

cases except for summertime Russia (see Fig. S6j), there is a dipolar structure of positive (negative) anomaly to the west (east) of the blocking center, consistent with the northward (southward) transport of moist (dry) air for the low (high) latitudes by the anticyclonic circulation.

To further explore the physics of the temperature anomalies (including the westward shift) and also the potential role of moisture, we start with the temperature tendency equation (Yanai et al. 1973; Yanai and Tomita 1998):

$$c_p \frac{\partial T}{\partial t} = c_p (-\mathbf{u}_h \cdot \nabla T + \omega \sigma) + Q_1, \quad (1)$$

where c_p is heat capacity and $\mathbf{u}_h = (u, v)$. Static stability σ is defined as $\sigma = -(T/\theta)(\partial\theta/\partial p)$ where p is pressure and θ is potential temperature. The first term on the right-hand side of Eq. (1) represents horizontal and vertical thermal advection,

North Pacific: Winter

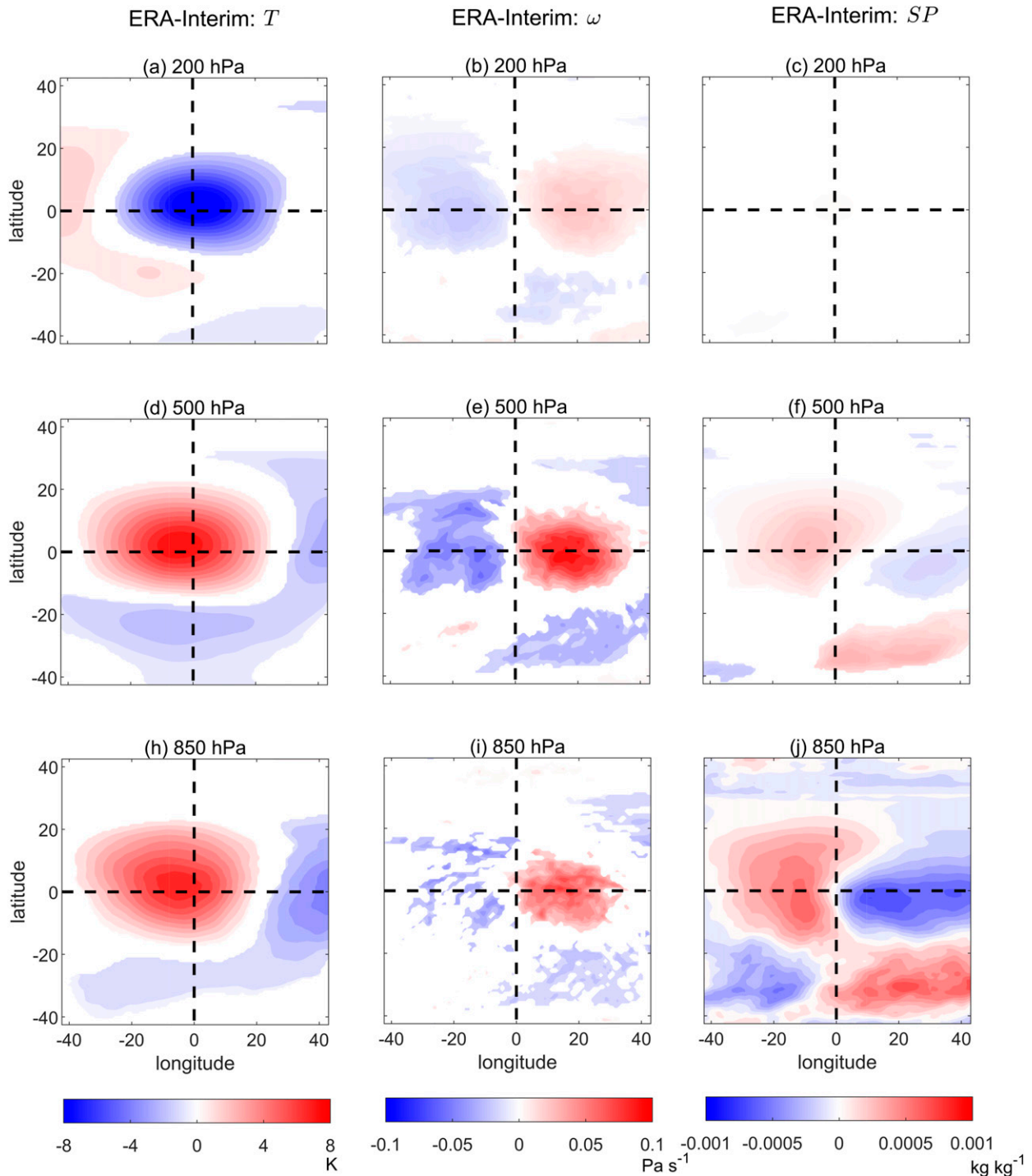


FIG. 2. Composites of anomalous temperature (T), vertical wind (ω), and specific humidity (SP) of blocking events in the ERA-Interim (1979–2019) over the North Pacific sector during winters (DJF). Rows show the (top) 200-, (middle) 500-, and (bottom) 850-hPa levels. Columns show (left) T , (center) ω , and (right) SP . In all panels, anomalies are first centered and then composited. The intersection of the dashed lines shows the center, and the latitudes and longitudes are relative to the center. All shown anomalies are significant at 95% level based on a one-sample t test.

North Pacific: Summer

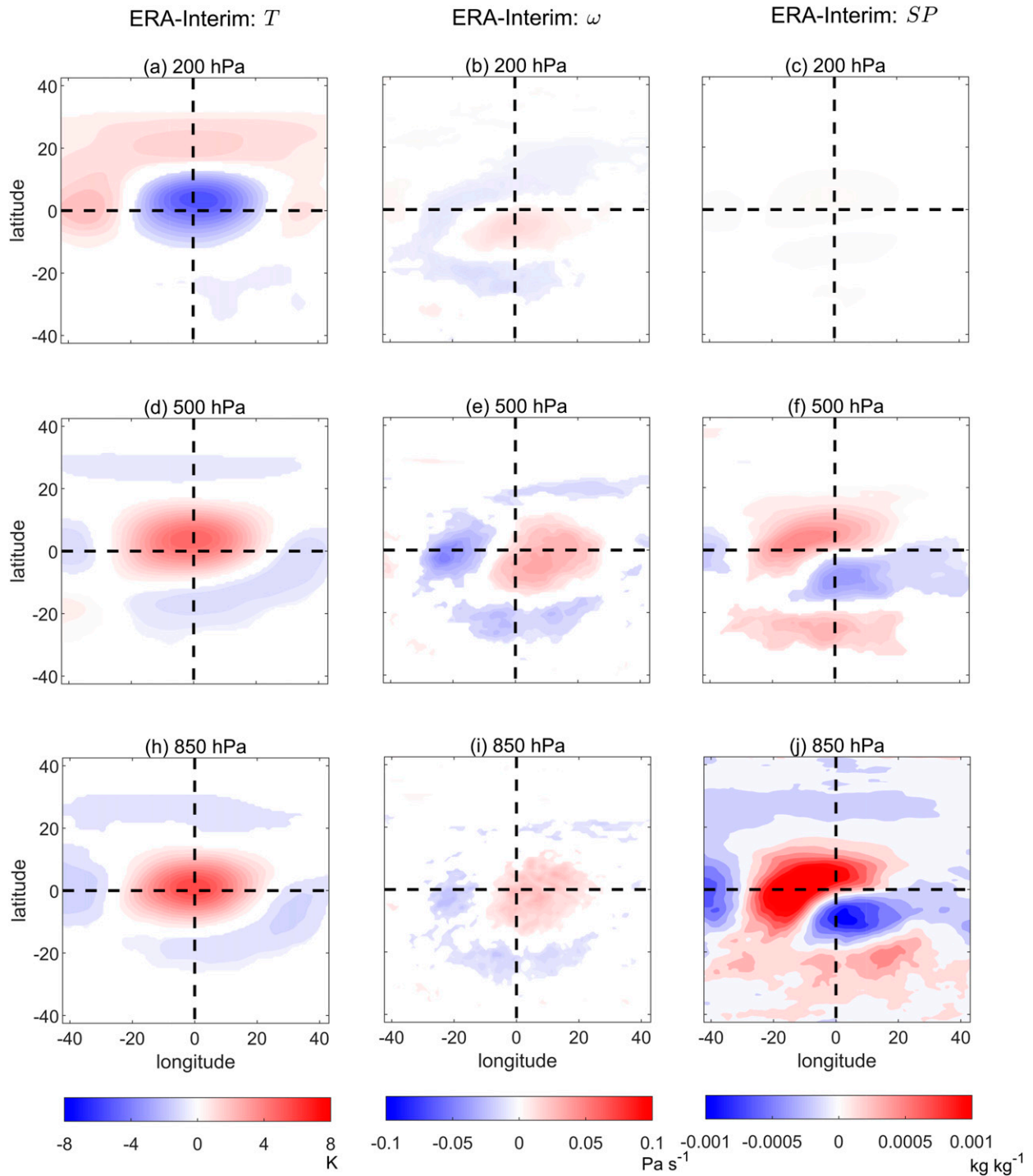


FIG. 3. As in Fig. 2, but for summers (JJA).

and the second term, Q_1 , represents heating due to radiation and latent heating due to net condensation. To better understand the role of moisture, the latter component of Q_1 (which itself is unavailable) can be quantified by calculating the apparent moisture sink Q_2 :

$$Q_2 = -L \frac{\partial \text{SP}}{\partial t} - L \left(\mathbf{u}_h \cdot \nabla \text{SP} + \omega \frac{\partial \text{SP}}{\partial p} \right), \quad (2)$$

where L is the specific latent heating (Yanai et al. 1973; Yanai and Tomita 1998). The term Q_2 represents latent heating due to net condensation (Yanai et al. 1973). Composites of anomalous horizontal and vertical components of thermal advection and of anomalous Q_2/c_p for winter and summer blocks over the North Pacific and Russia at 500 and 850 hPa are shown in Fig. 4 (winter) and Fig. 5 (summer). Results for the North Atlantic sector are shown in Fig. S7. Note that in Figs. 4 and 5 and Fig. S7, we first calculate each term using the 6-hourly¹ full-field variables and then remove each term's climatology using a 31-day centered moving average to calculate the corresponding anomalous field (Ueda et al. 2003; Hsu and Li 2011; Li et al. 2017). Finally, the anomalous fields are centered and composited as described in section 2.

Consistent among both seasons and three sectors, there is substantial adiabatic warming around the blocking centers, with a major contribution from vertical advection (i.e., the $\sigma\omega$ term); see the first three columns of Figs. 4 and 5 and Fig. S7. This warming by descending flow in some cases (e.g., both seasons of the North Pacific and North Atlantic sectors) is slightly shifted to the east, due to the dipolar pattern of ω mentioned earlier. The contribution of horizontal advection has some seasonal and regional dependencies: either it is small or it consists of warming on the western and cooling on the eastern side of the blocking event (dominated by meridional advection). Using the maximum amplitude of the warming anomaly as a measure of strength, for all three regions, the total adiabatic warming is overall stronger around 850 hPa (compared to 500 hPa) in winters, particularly over ocean basins, but slightly stronger around 500 hPa over summers, particularly over Russia (see the captions of Figs. 4 and 5 and Fig. S7 for the values).

The anomalous Q_2 pattern also shows some seasonal and regional dependencies: it is either dipolar with a negative anomaly on the eastern and a positive anomaly on the western side of the blocks, or it is monopolar with a negative anomaly around the blocking center. Note that all these figures show the Q_2 anomaly; therefore, negative values mean *anomalously below-normal* latent heating. Also, examining the contributions from different terms of Eq. (2) shows that overall, Q_2 is mainly dominated by vertical advection of SP (i.e., the $\omega\partial\text{SP}/\partial p$ term). Using the maximum amplitude of the negative anomaly as a measure of strength, Q_2 is always stronger around 850 hPa (compared to 500 hPa) and at this level is overall as strong as total adiabatic warming in summers but weaker than total

adiabatic warming in winters, particularly over the ocean basins (see the captions of Figs. 4 and 5 and Fig. S7 for the values). Below we further discuss some of the seasonal and regional dependencies of the adiabatic warming and latent heating.

In winters of North Pacific and North Atlantic, in addition to the warming around the center mentioned above, there is cooling (warming) on the southern/eastern (western) side of the blocks; see Figs. 2d,h and Figs. S3d,h. The anomalous cooling on the southern/eastern side is due to a combination of horizontal thermal advection (dominated by meridional advection from higher latitudes), vertical advection, and the east–west dipolar structure of anomalous Q_2 (Figs. 4a–h and Figs. S7a–h). The anomalous warming on the western side of these blocks is due to latent heating, that is, the anomalously positive Q_2 on the western side (Figs. 4d,h and Figs. S7d,h). Using an alternative approach to quantifying the contribution of latent heating based on the parameterization in Lackmann (2002) leads to (qualitatively) the same conclusion about the role of latent heating in the anomalous warming on the western side of these blocking events (not shown).

These findings are also consistent with those of Steinfeld and Pfahl (2019), where the contribution of latent heating (upstream) is found to be large for blocks over the oceans during NH winters. Our analysis suggests that the westward shift of T (which we noted earlier), particularly in the winter of North Pacific, is due to latent heating. This is further confirmed using idealized modeling experiments. Figure S8 shows the longitude–pressure (as well as latitude–pressure) composites of T anomalies for blocking events simulated in the idealized dry GCM (Fig. S8a) and the summer (Fig. S8b) and winter (Fig. S8c) of the idealized moist GCM. The structure of T anomaly is aligned with the blocking center in the dry case while there is a westward shift in the moist case, most notably in winters when latent heating has a stronger effect.

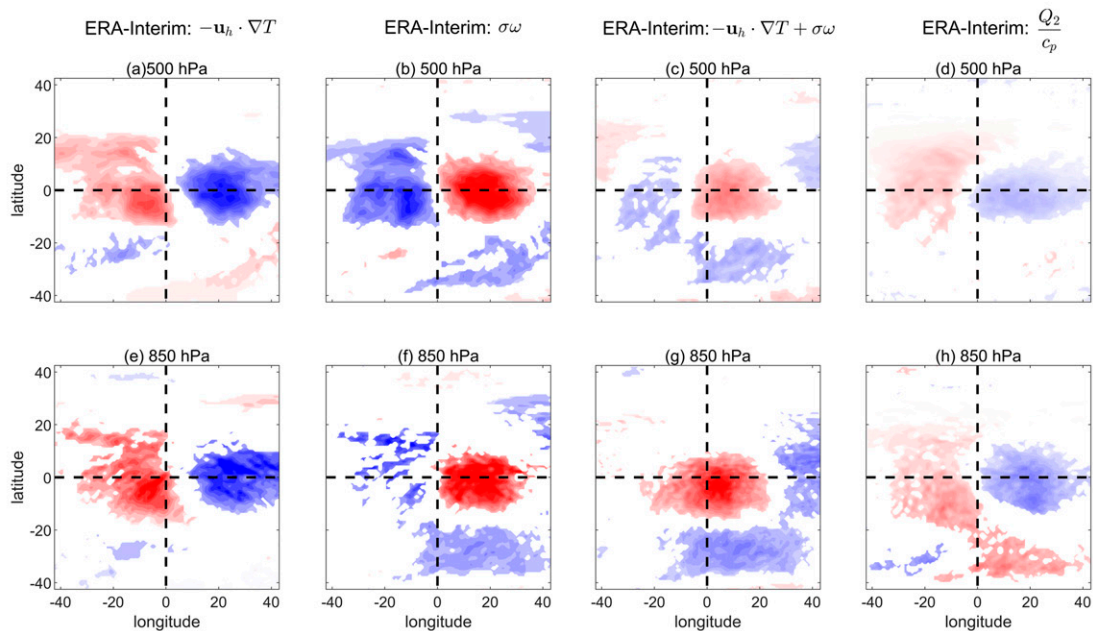
In winters over Russia, horizontal thermal advection has a small contribution compared to vertical advection except in the southeast side of the blocks, where it leads to cooling particularly around 850 hPa (Figs. 4m,o), consistent with the cold anomaly in Fig. S5h. Furthermore, the Q_2 anomaly is negative and has a monopolar structure around the center (Figs. 4i–p), canceling out the adiabatic warming due to vertical advection. As a result, the structure of T is a positive anomaly around the center and a negative anomaly on the southeast side of blocks. Due to monopolar structure of Q_2 , the T anomaly does not have the westward shift.

During summer, in addition to the adiabatic warming around the blocking centers due to vertical advection in all the three sectors, there is anomalously weak cooling on the eastern side due to meridional advection and an anomalously negative Q_2 pattern around the center and to the east. Contribution of upstream latent heating is larger over Russia during summer compared to winter, where latent heating is insignificant (Figs. 5l,p). This is in agreement with the results of Steinfeld and Pfahl (2019) and Zschenderlein et al. (2019), who found that in summers there are some contributions from latent heating in the up-stream regions of continental blocks.

In short, aside from the dominant role of adiabatic warming by vertical advection in all sectors and both seasons,

¹ We have also repeated this analysis with daily-averaged variables and found very similar results.

North Pacific: Winter



Russia: Winter

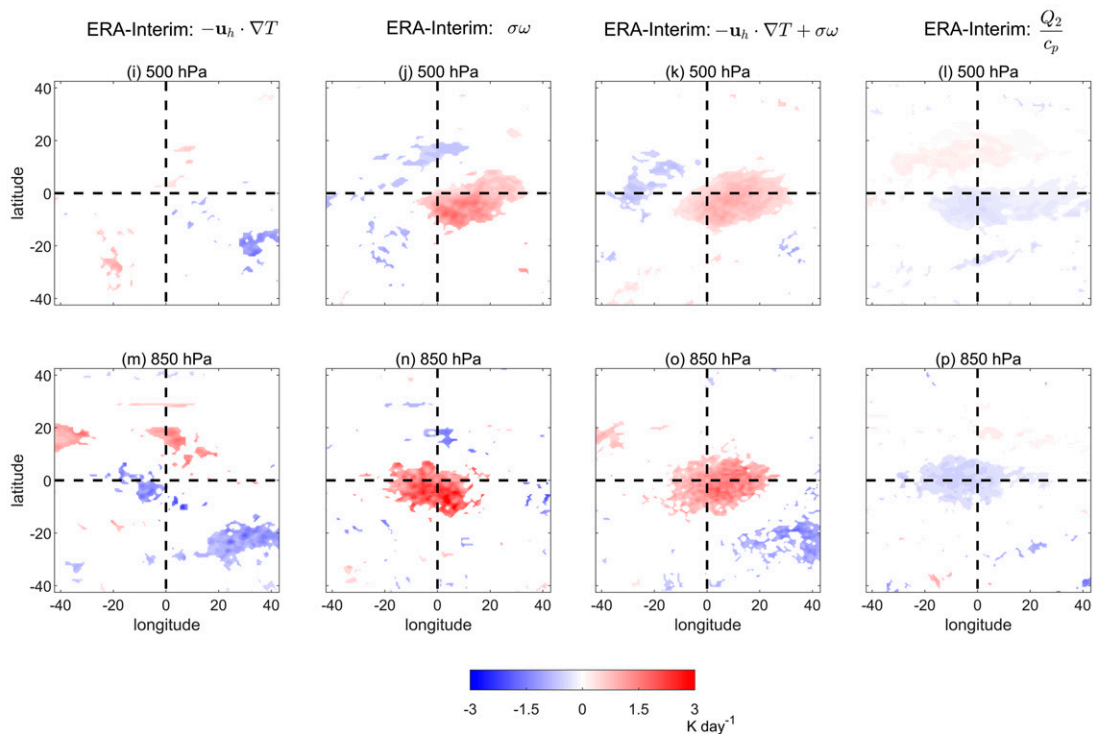
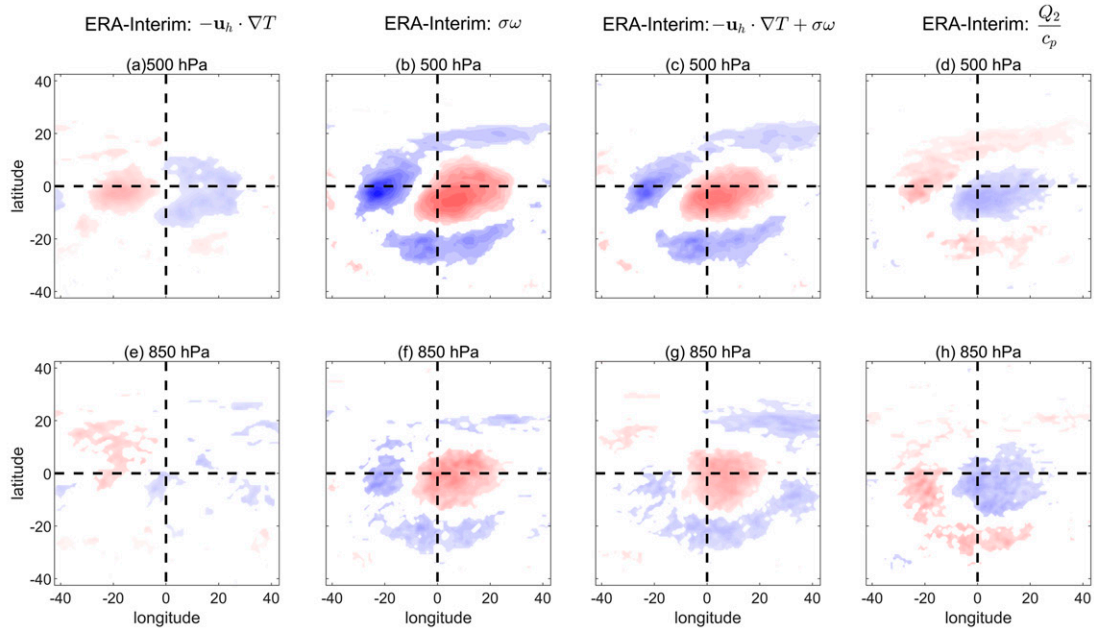


FIG. 4. Composites of (first column), (second column) anomalous wintertime horizontal and vertical components of adiabatic warming, (third column) total adiabatic warming, and (fourth column) latent heating of blocking events over the North Pacific and Russia in the ERA-Interim (1979–2019). All shown anomalies are significant at 95% level based on a one-sample t test. The maximum amplitude of total adiabatic warming over North Pacific is 1.68 K day^{-1} (500 hPa) and 3.32 K day^{-1} (850 hPa) and over Russia is 1.34 K day^{-1} (500 hPa) and 2.2 K day^{-1} (850 hPa). The maximum amplitude of negative Q_2 anomaly (i.e., below-normal latent heating) over North Pacific is -0.86 K day^{-1} (500 hPa) and -1.62 K day^{-1} (850 hPa) and over Russia is -0.69 K day^{-1} (500 hPa) and -1.68 K day^{-1} (850 hPa).

North Pacific: Summer



Russia: Summer

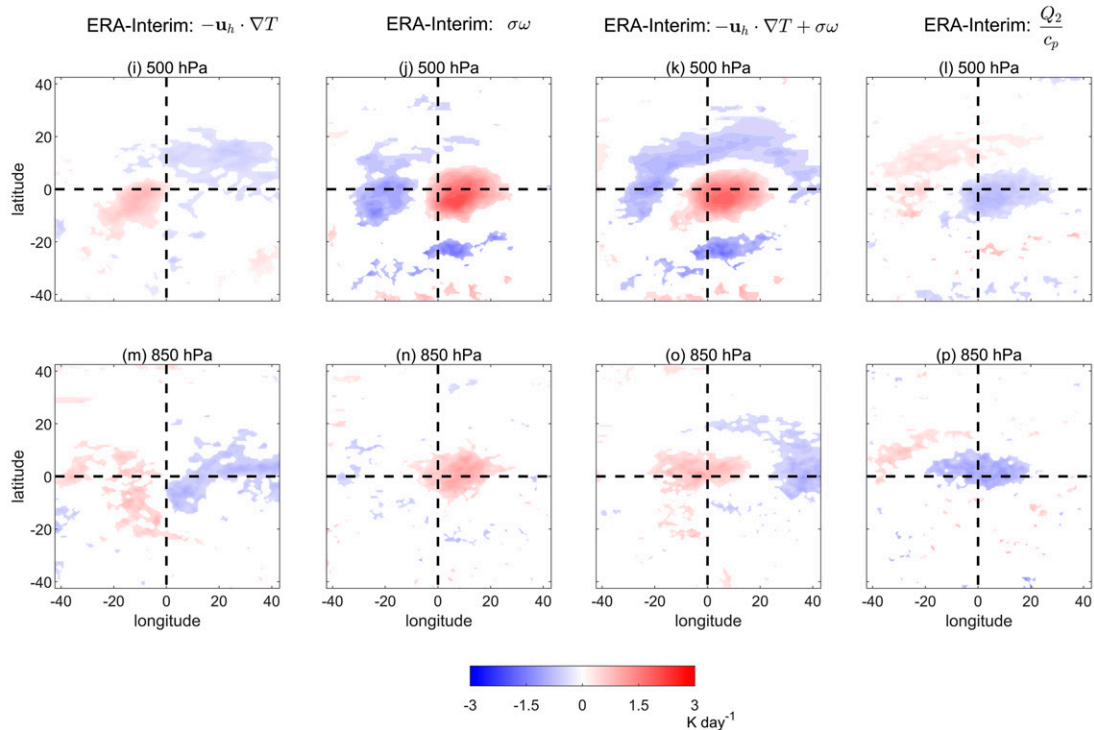


FIG. 5. Composites of (first column),(second column) anomalous summertime horizontal and vertical components of adiabatic warming, (third column) total adiabatic warming, and (fourth column) latent heating over the North Pacific and Russia in the ERA-Interim (1979–2019). All shown anomalies are significant at 95% level based on a one-sample *t* test. The maximum amplitude of total adiabatic warming over North Pacific is 1.69 K day^{-1} (500 hPa) and 1.15 K day^{-1} (850 hPa) and over Russia is 1.94 K day^{-1} (500 hPa) and 1.20 K day^{-1} (850 hPa). The maximum amplitude of negative Q_2 anomaly (i.e., below-normal latent heating) over the North Pacific is -0.90 K day^{-1} (500 hPa) and -1.02 K day^{-1} (850 hPa) and over Russia is -0.80 K day^{-1} (500 hPa) and -1.22 K day^{-1} (850 hPa).

contributions of horizontal adiabatic warming and latent heating vary by region and season. Understanding the reasons behind these dependencies require further analysis of the regional and seasonal background flows and temperature fields as well as the physics giving rise to dipolar versus monopolar blocks' ω structure (which is associated with the Q_2 and adiabatic warming patterns). While such analysis is beyond the scope of this paper, we hope that our findings motivate future work.

Finally, the cold anomaly in lower stratosphere that is seen in all cases (also clearly seen in the idealized dry and moist GCMs; Fig. S8) is a natural consequence of the lifted tropopause associated with the negative PV anomaly and is consistent with the blocks' wind anomalies through the thermal wind balance. For example, on the poleward and eastern sides of the block, anomalous u and v are, respectively, eastward and southward and increase in magnitude from the surface to near the tropopause, above which the magnitude declines. As a result, $\partial u/\partial p < 0$ and $\partial v/\partial p > 0$ in the troposphere, leading to $\partial T/\partial y$ and $\partial T/\partial x$ that are negative, thus a positive T anomaly under the anticyclone. In the lower stratosphere, $\partial u/\partial p > 0$ and $\partial v/\partial p > 0$, leading to positive $\partial T/\partial y$ and $\partial T/\partial x$, thus a negative T anomaly above the anticyclone (examining the wind anomalies and thermal wind balance on the equatorward and western sides of the block leads to the same results). For the same reason, a similar cold anomaly in the lower stratosphere above a warm anomaly in the troposphere is seen in the pattern of the temperature anomaly associated with the leading EOF of zonal-mean zonal wind (i.e., the annular mode) in both hemispheres (Thompson and Li 2015; Ma et al. 2017; Hassanzadeh and Kuang 2019).

b. Large-ensemble fully coupled GCM simulations

Before using the simulations in the LENS and GFDL-LE datasets to understand how the 3D structure of blocking events might respond to climate change, here we aim to examine how well these models reproduce the climatology of the blocking events' 3D structure. Figures 6 and 7 show the 1981–2005 climatology of the 3D structure of wintertime and summertime North Pacific blocking events in LENS using the same variables used from reanalysis (except for ω , Z200, and Z850, which were not available). Figures S9–S12 show similar results but for the North Atlantic and Russian sectors. Comparing these results with those from reanalysis (Figs. 1–3 and S1–S6) shows that the NCAR's CESM1 model reproduces the patterns and amplitudes associated with the 3D structure of blocking events faithfully over all three sectors and in both summers and winters. In particular, the complex patterns of T and SP anomalies and the regional and seasonal dependencies discussed earlier (e.g., the westward shift of T) are well reproduced by the model. One exception might appear to be the pattern of T in summers at 500 and 850 hPa over all regions, which includes broad cooling regions around the central warming region of the blocks in the model but not in reanalysis. However, a closer examination of the reanalysis data shows that similar broad cooling exists but not at the 95% level used for statistical significance here.

Analysis of the GFDL-LE dataset (no shown) demonstrates that the GFDL CM3 model reproduces the climatology of the

blocking events' 3D structure similarly well (note that the daily SP and ω fields were not available for examination).

The above findings, namely that CEMS1 and GFDL CM3 fully coupled models reproduce the climatology of the 3D structure of blocking event very well, are interesting given that these models are known to have biases in reproducing the climatological NH large-scale circulation (Kwon et al. 2018; Athanasiadis et al. 2020) and are known to underestimate blocking frequency (Lee and Ahn 2017; Kwon et al. 2018; Athanasiadis et al. 2020), which is a persistent bias in generations of comprehensive climate models (Barnes et al. 2012; Davini and Cagnazzo 2014; Lee and Ahn 2017; Matsueda and Endo 2017; Jiang et al. 2019; Simpson et al. 2020). This issue will be further discussed in the next section.

4. Response of the blocking events' 3D structure to climate change

In this section, we study the response of the 3D structure of blocking events to climate change using the two large-ensemble datasets. To compute the response of each variable, we first calculate the composited anomaly in the current and future climates, separately, and then calculate the difference (as future minus current). This approach has been used recently in some studies of Euro-Atlantic blocking events (Masato et al. 2014; Kennedy et al. 2016). We start with the response in summers and then discuss the response in winters.

a. Summer (JJA)

The responses of the blocking events' Z500 field over the three sectors in summers are shown in Fig. 8 (the two left columns). Both models predict a weakening of Z500 around the blocking center over all three regions, although the decline is much stronger in the GFDL CM3 model (and in LENS over North Atlantic, there is small strengthening of Z500 on the sides). Examining the tropospheric u response (Fig. S13) demonstrates a robust weakening at both 850 and 500 hPa in both models and all regions, consistent with the overall decrease in Z500. Figures 9 and 10 show responses of temperature anomalies in the LENS and GFDL-LE datasets, respectively. At 200 hPa, consistent among models and regions, there is a positive response (i.e., weakening of the blocking events' cold temperature anomaly in the lower stratosphere). Both models also predict cooling in the troposphere (i.e., weakening of the blocks' temperature anomaly) with three exceptions: the response of T at 850 hPa over the North Atlantic and Russia in LENS is positive while over North Atlantic in GFDL-LE it is near zero around the blocking center (Figs. 9h,i and 10h,i).

To understand what causes this discrepancy between the model predictions, we analyze the results of self-organizing map (SOM; Kohonen 2012) clustering of blocking events over the North Atlantic and Russian sectors in the reanalysis and in the two models. Here, we have clustered Z500 anomalies associated with blocking events in the current climate into two distinguishable clusters using a map of 2×1 nodes [the SOM algorithm and details are the same as those described in Hassanzadeh et al. (2020)]. As shown in Fig. S15, the GFDL CM3 model accurately

North Pacific: Winter

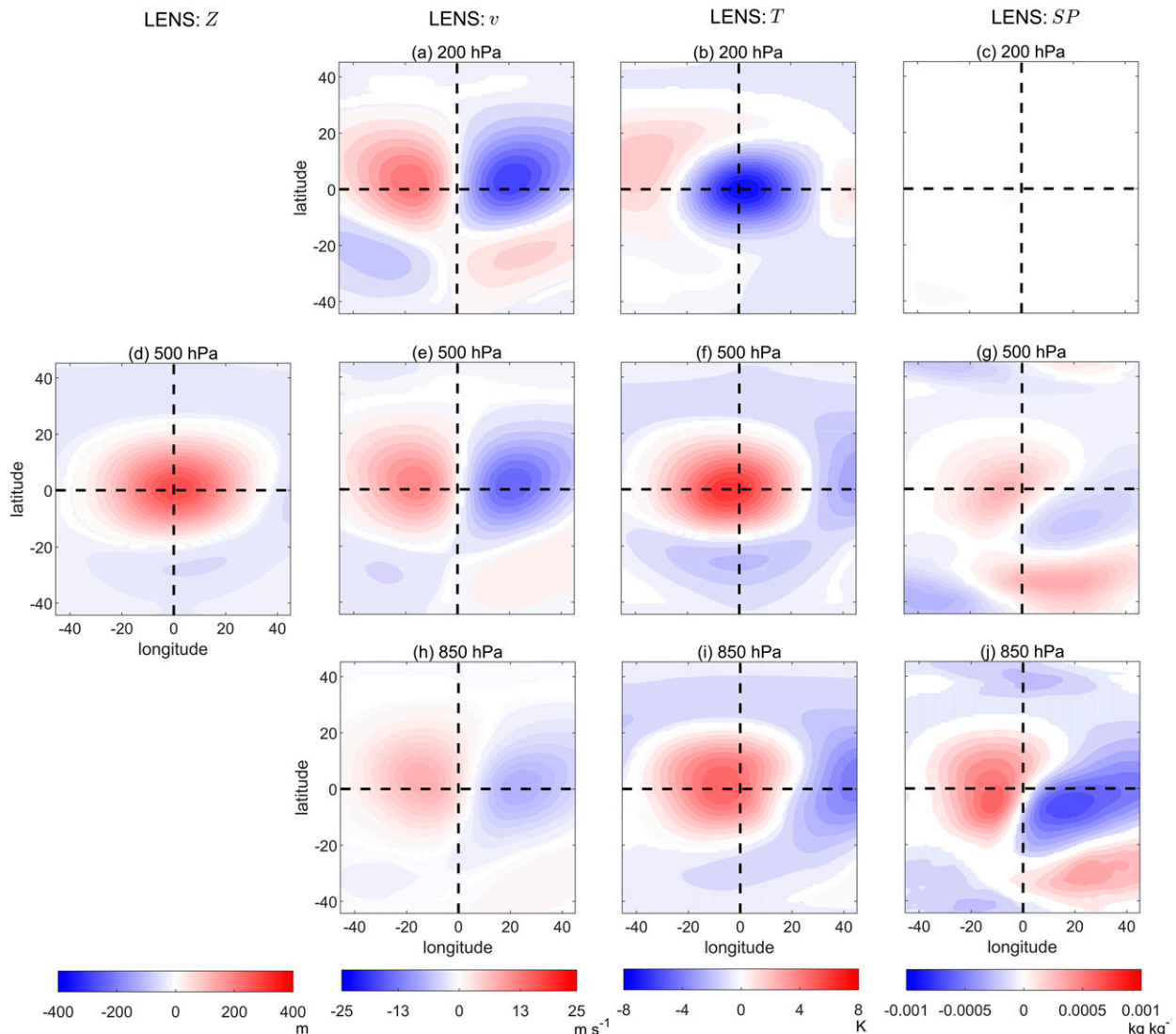


FIG. 6. Composites of anomalous (left to right) Z500, meridional wind (v), temperature T , and specific humidity SP of wintertime (DJF) blocking events in LENS over the North Pacific sector from 1981 to 2005. Rows show (top) 200-, (middle) 500-, and (bottom) 850-hPa levels. Daily Z200 and Z850 are not available in the LENS dataset. In all panels, anomalies are first centered in and then composited. The intersection of the dashed lines shows the center, and the latitudes and longitudes are relative to the center. All shown anomalies are significant at 95% level based on a one-sample t test.

captures the frequencies and locations/patterns of clusters over Scandinavia and the Atlantic Ocean. However, the CESM1 model does not capture the frequencies of these two separate classes, and the locations/patterns are not entirely the same as those in the reanalysis. Further analysis (not shown) shows that cluster 1 in the LENS dataset, which is overestimated, has a strongly positive T response at the low levels, resembling the total positive response in Fig. 9h. A similar clustering analysis has been performed over Russia. Although both models are relatively able to capture the frequencies and patterns of blocking events in the current over this sector, their future

locations/patterns are entirely different (Fig. S16), which leads to different responses in T (and other fields). Overall, the temperature anomalies associated with summertime blocking events are projected to weaken under climate change, except over Russia where there is disagreement among the two models.

It should be noted that these apparent weakenings of the Z500 and T anomalies do not necessarily mean weakening of the impact of blocking events in the future. While the response of blocking events over North Atlantic (and perhaps Russia) seems less trustworthy in LENS, this dataset provides daily

North Pacific: Summer

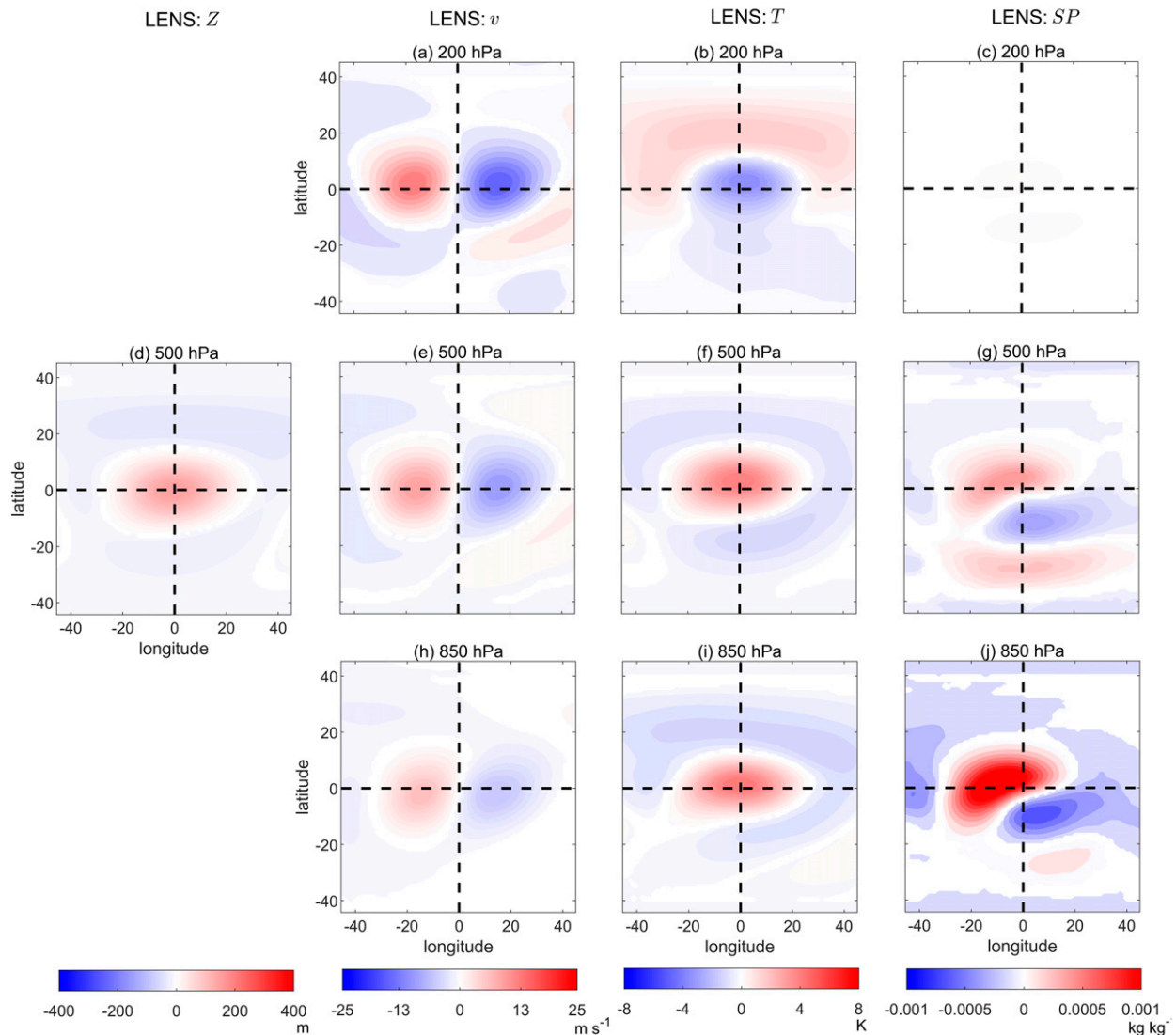


FIG. 7. As in Fig. 6, but for summers (JJA).

near-surface air temperature (T2m). With this caveat in mind, Fig. 11 shows the response of T2m associated with blocking events. Over Russia (Fig. 11e), where the T2m anomaly is already the largest (and positive), the predicted response is positive near the blocking center, further amplifying the impact of future heat waves over this region, which is consistent with the results of Galfi and Lucarini (2021) over land. The response over the ocean basins is more complex, but there are both anomalous cooling and warming under the block. Note that the sign of the response in the near-surface temperature depends on factors beyond just the change in the strength of the blocking events; examples of other factors are changes in the large-scale background zonal and meridional temperature gradients (Schneider et al. 2015; Holmes et al. 2016) and over land, changes in the soil–moisture feedback (Fischer et al.

2007; Hauser et al. 2016; Rasmijn et al. 2018). To gain a deeper understanding, further analyses in the future studies, particularly using large-ensemble model outputs that include daily (or subdaily) ω and SP, are needed.

In contrast to other variables discussed so far, the SP anomaly associated with the blocking events is projected to strengthen in future summers (Fig. 12; only for LENS, in which daily SP was available). Over the two ocean basins, and particularly at 850 hPa over North Pacific, the response of SP is generally positive (negative) on the western (eastern) side, reinforcing the SP anomaly associated with the blocking events. Over Russia, the response is mainly negative on the eastern side and around the center and to a lesser degree positive on the western side, but again strengthening the SP anomaly.

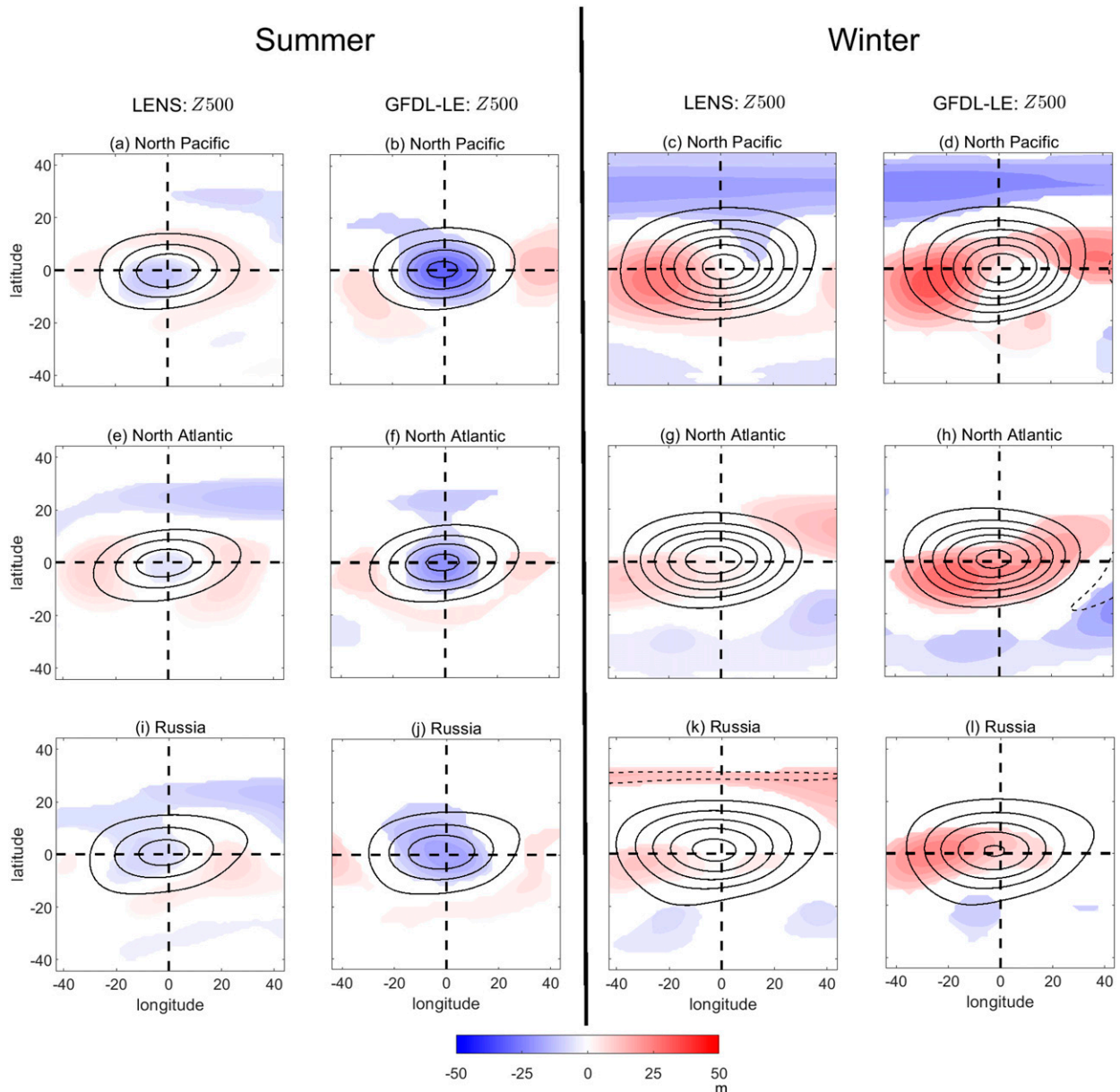


FIG. 8. Response of the blocking events' Z500 in (left) summer (JJA) and (right) winter (DJF) in the LENS and GFDL-LE datasets, for the (a)–(d) North Pacific sector, (e)–(h) North Atlantic sector, and (i)–(l) Russian sector. All shown anomalies are significant at 95% level based on a two-tailed t test. Contour lines represent the climatology of Z500 anomalies with the interval of 50 m.

To summarize, the response of summertime blocking events to climate change is, overall, weakening of Z500, wind, and T anomalies and strengthening of SP anomalies, although the responses are much stronger in GFDL-LE, and the two models disagree over the sign of the low-level T response over Russia.

b. Winter (DJF)

The responses of the blocking events' Z500 field over the three sectors in winters are shown in Fig. 8 (the two right columns). Both models agree on the strengthening of Z500 over North Pacific (first row). Over North Atlantic and Russia, GFDL CM3 predicts strengthening of Z500 while CESM1

predicts small responses (although positive and statistically significant). Overall, the responses in Z500 are positive but, unlike in summer, spatially nonuniform, and often shifted westward (more discussion to follow). These results are consistent with those of Kennedy et al. (2016), who found that the Z500 anomalies of European blocks nonuniformly strengthen in the future. Consistent with the Z500 responses, examining the tropospheric u response (Fig. S14) shows clear strengthening in all three sectors in GFDL-LE and in North Pacific in LENS, but a more complicated response in the other two sectors.

Figures 13 and 14 show responses of temperature anomalies in the LENS and GFDL-LE datasets, respectively. Like

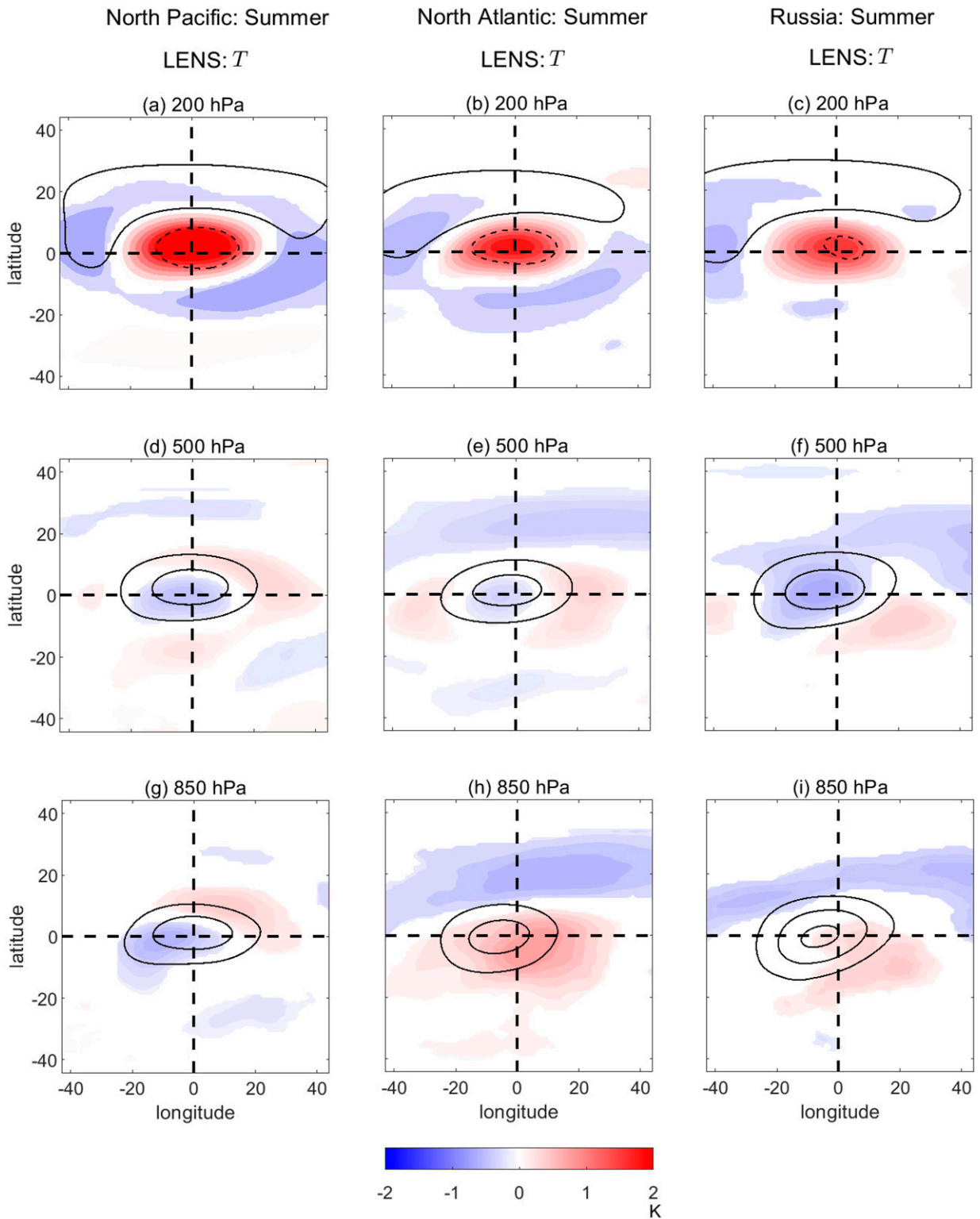


FIG. 9. Response of summertime (JJA) temperature T associated with blocking events in the LENS dataset. Rows show the (top) 200-, (middle) 500-, and (bottom) 850-hPa levels. Columns show the (left) North Pacific, (center) North Atlantic, and (right) Russian sectors. All shown anomalies are significant at 95% level based on a two-tailed t test. Contour lines represent the climatology of T anomalies with the interval of 2 K.

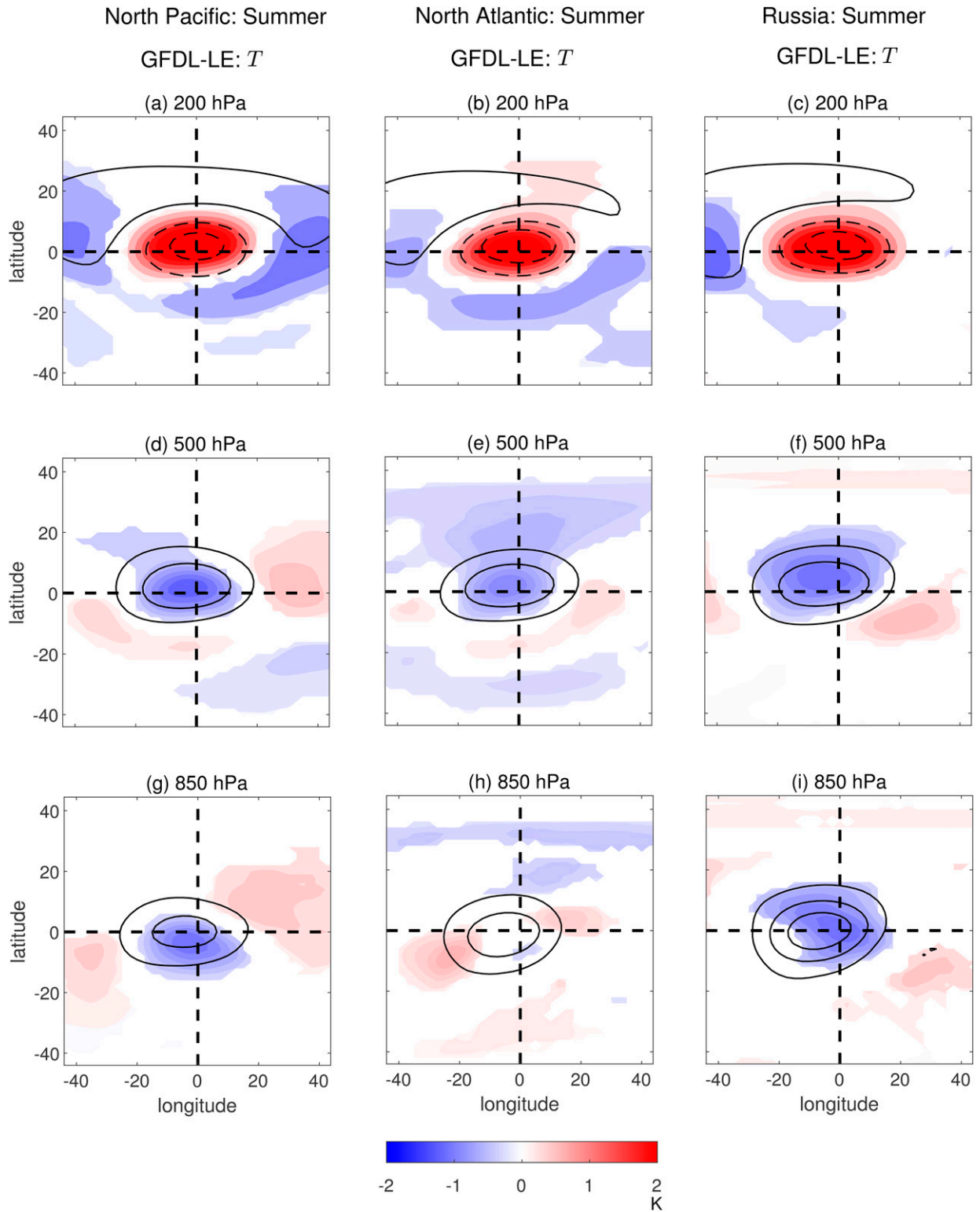


FIG. 10. As in Fig. 9, but for the GFDL-LE dataset.

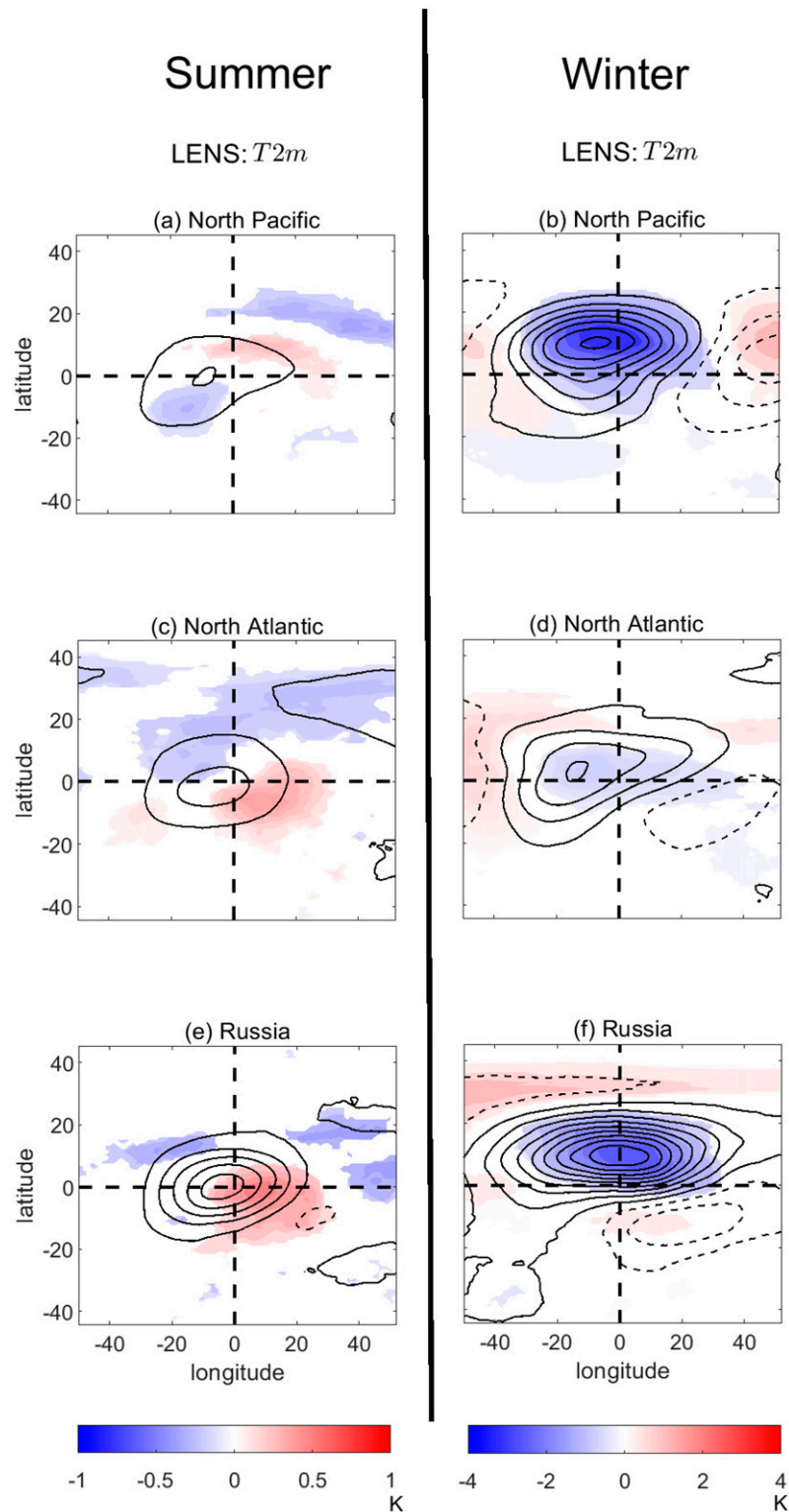


FIG. 11. Response of (a),(c),(e) summertime (JJA) and (b),(d),(f) wintertime (DJF) near-surface surface temperature T_{2m} associated with blocking events in the LENS dataset. Rows show the (top) North Pacific, (middle) North Atlantic, and (bottom) Russian sectors. All shown anomalies are significant at 95% level based on a two-tailed t test. Contour lines represent the climatology of T_{2m} anomalies with the interval of 1 K.

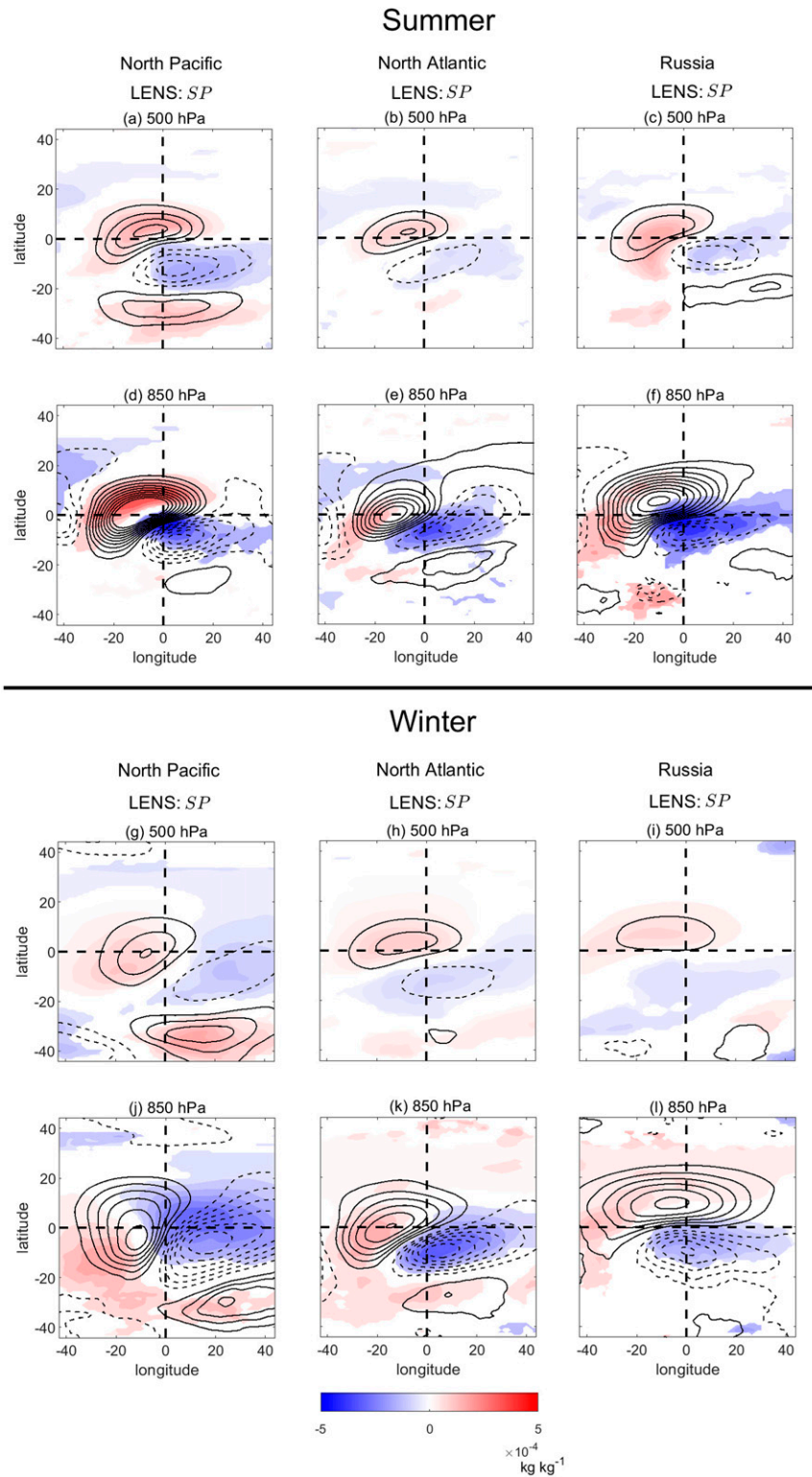


FIG. 12. Response of (a)–(f) summertime (JJA) and (g)–(l) wintertime (DJF) specific humidity (SP) associated with blocking events in the LENS dataset. Rows show the results at (a)–(c),(g)–(i) 500 and (d)–(f),(j)–(l) 850 hPa. Columns show the (left) North Pacific, (center) North Atlantic, and (right) Russian sectors. All shown anomalies are significant at 95% level based on a two-tailed t test. Contour lines represent the climatology of SP anomalies with the interval of 10^{-5} kg kg⁻¹.

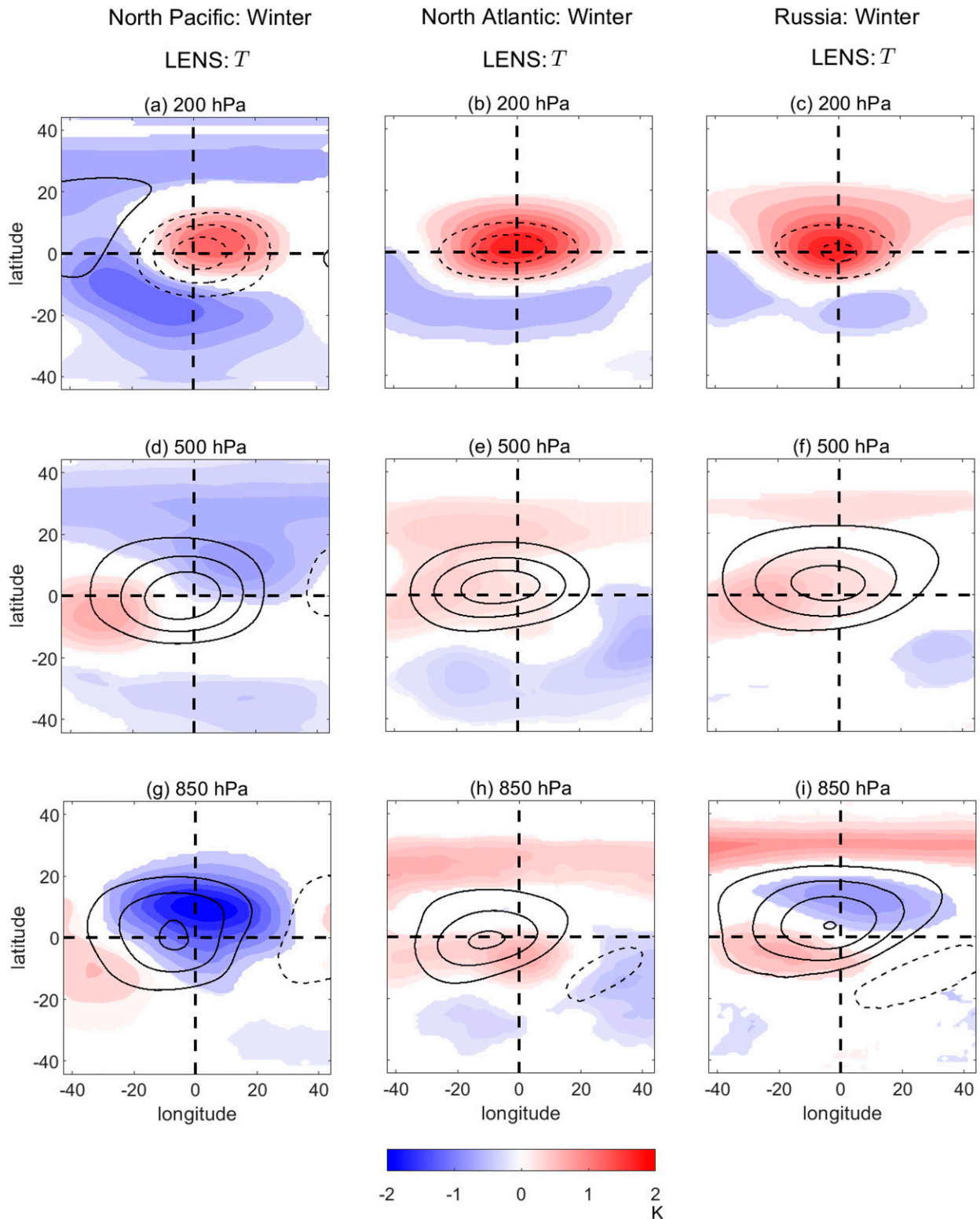


FIG. 13. Response of wintertime (DJF) temperature T associated with blocking events in the LENS dataset. Rows show the (top) 200-, (middle) 500-, and (bottom) 850-hPa levels. Columns show the (left) North Pacific, (center) North Atlantic, and (right) Russian sectors. All shown anomalies are significant at 95% level based on a two-tailed t test. Contour lines represent the climatology of T anomalies with the interval of 2 K.

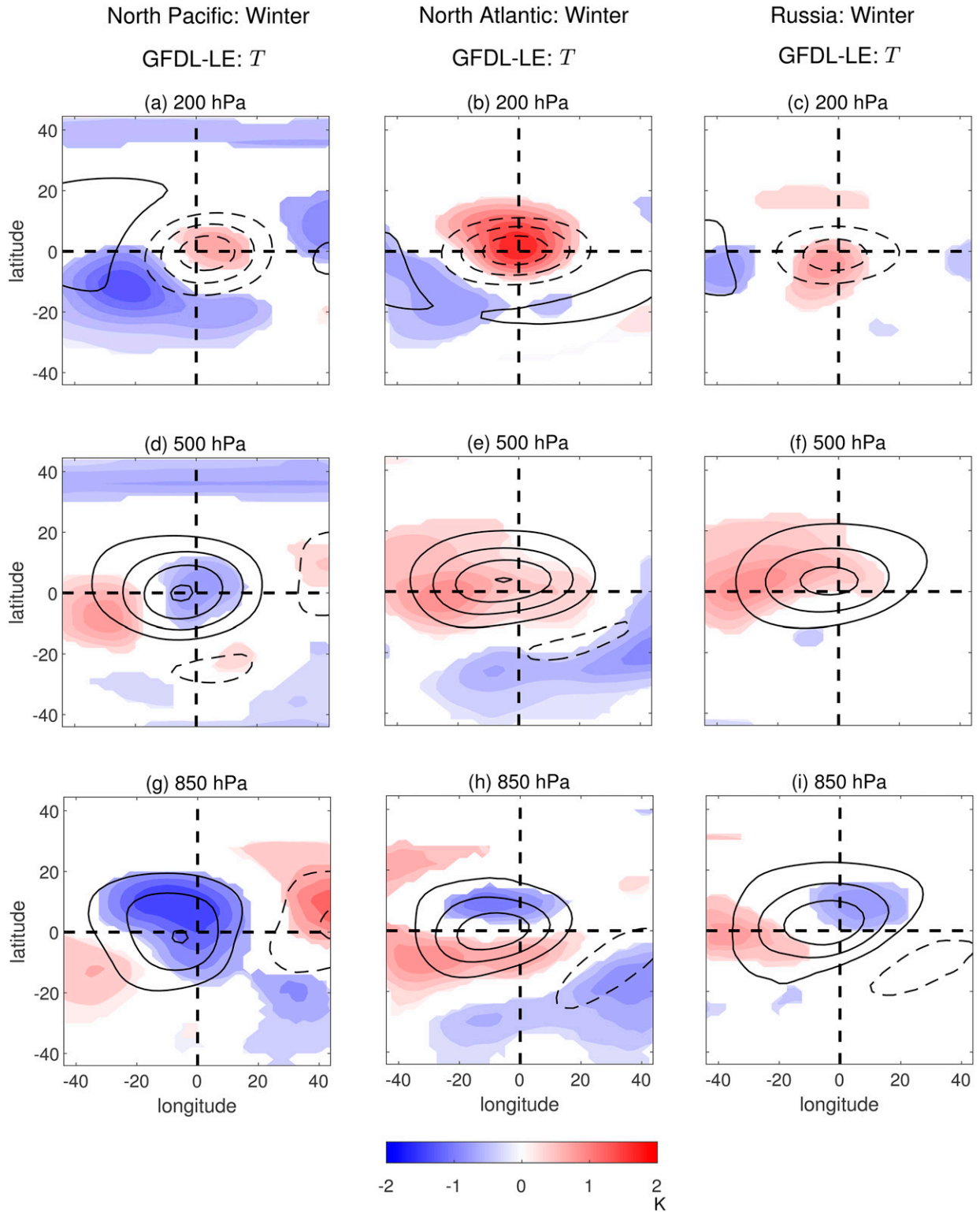


FIG. 14. As in Fig. 13, but for the GFDL-LE dataset.

summertime responses, both models predict warming at 200 hPa, which weakens the cold T anomaly associated with blocking events in lower stratosphere (Figs. 13a–c and 14a–c). Over North Pacific, both models agree on substantial cooling at 850 hPa and some cooling at 500 hPa, although there is also weak warming on the western sides on both levels (Figs. 13d,g and 14d,g). Over Russia, both models predict westward-shifted warming at 500 hPa and cooling near the center and warming on the western side at 850 hPa (Figs. 13f,i and 14f,i). Finally, over the North Atlantic, while both models show warming around the center and western side at 500 hPa, they do not agree on the sign of the response at 850 hPa (Figs. 13h and 14h).

The response of SP anomaly associated with blocking events shows strengthening over all three sectors, especially over the North Pacific and North Atlantic (Fig. 12). Over these two ocean sectors, there is positive (negative) SP response on the western (eastern) side of the blocking center. These results suggest that increased latent heating, due to increased low-level moisture, is likely responsible for the positive T response on the western side, which is associated with the noticeable westward-shifted strengthening of Z500 mentioned earlier (Fig. 8). Confirming this connection requires future work using large-ensemble model outputs (including ω and SP) with sub-daily sampling such that the temperature tendency equation could be thoroughly analyzed (as done in section 3).

Finally, the weakening of the low-level T anomalies in winter is also manifested in the weakening of T2m associated with blocks over North Pacific, Russia, and even North Atlantic (Fig. 11). The latter is consistent with the results of Kennedy et al. (2016) and Masato et al. (2014).

5. Discussion and summary

In this paper, we present a composite analysis of current and future NH blocking events' 3D structure by analyzing geopotential height, 3D velocity field, temperature, and specific humidity, and in some cases their connections, at three levels: 200, 500, and 850 hPa. We aim to answer four specific questions, which are listed in the introduction.

With regard to question 1, which is about the climatology of blocking events, the reanalysis data show that over both ocean and land and in both seasons, the anomalous anticyclonic winds are equivalent-barotropic in the troposphere and stratosphere, and the temperature anomalies are positive throughout the troposphere and negative in the lower stratosphere. The main seasonal and regional differences are that blocks are larger and stronger in winters, and over oceans, the temperature anomaly is shifted westward, most noticeably in winters. Further analysis shows that this westward shift, which is reproduced even in an idealized moist GCM, is due to latent heating on the upstream region of blocking events. Overall, there is subsidence near the blocking center, although in some cases (e.g., over North Pacific) this descending branch is shifted eastward and accompanied by an equally strong ascending branch to the west, creating a dipolar structure for ω . In general, the findings about the climatology (including the westward shift and role of latent heating) are consistent with those reported in various earlier papers, which were mainly focused on case studies or

composites of blocking events over ocean (e.g., Mak 1991; Brunner and Steiner 2017; Steinfeld and Pfahl 2019).

To address question 2, which is about the physics driving the positive temperature anomaly under the anticyclone, we quantify the contributions of horizontal and vertical thermal advection and latent heating due to net condensation (Q_2) in the temperature tendency equation using reanalysis data. Consistent among both seasons and three sectors, we find adiabatic warming due to subsidence as a major contributor to warming near the center of blocking events, although the warming could be slightly shifted eastward when ω has a dipolar structure. Depending on the season, region, and level, meridional advection and Q_2 can also have leading-order contributions to the thermal budget under the anticyclone. For example, for wintertime North Pacific blocks, at 850 hPa, the total adiabatic warming (due to both vertical and meridional advection) is much stronger than Q_2 , but the upstream latent heating still leads to the noticeable westward shift of T anomaly. As another example, in summertime Russian blocks, the 850-hPa total adiabatic warming (dominated by vertical advection) and anomalously negative Q_2 (i.e., below-normal latent heating) around the center and anomalously positive Q_2 (i.e., above-normal latent heating) on the west have comparable magnitudes. Overall, these findings, particularly on the dominant role of adiabatic warming due to subsidence and the importance of latent heating, are consistent with those recently reported for European blocks/heat waves and/or using Lagrangian trajectory analysis (e.g., Steinfeld and Pfahl 2019; Zschenderlein et al. 2019).

With regard to question 3, we find that both CESM1 and GFDL CM3 can reproduce the climatological 3D structure of blocking events, including the patterns of temperature and specific humidity anomalies, over all three sectors and in both seasons remarkably well. That said, we also find through clustering analysis that CESM1 (unlike GFDL CM3) does not reproduce the relative frequency and location of blocks over Atlantic Ocean versus Scandinavia well, leading to disagreements with GFDL-CM3 on the future response over the North Atlantic sector.

To address question 4, about the response of the 3D structure to climate change, we examine the difference in the composites of the anomalies at the end of the twenty-first century versus the end of the twentieth century under RCP8.5. We find both models to overall agree on the sign of the response, although there are a few disagreements, and responses are generally stronger in GFDL-LE compared to LENS. In summers, we find a general weakening of all anomalous fields, except for the specific humidity anomaly, which becomes stronger. However, in LENS, which provides daily 2-m air temperature, we find that this weakening does not necessarily translate to a weakening of the impact on near-surface temperature extremes. Most notably, the warm temperature anomaly associated with Russian blocking events is projected to intensify. Note that this increase in near-surface positive temperature anomaly, in spite of the apparent weakening of the block, is not because of the increase in the mean surface temperature due to climate change (since anomalies in each time period are computed with respect to the climatology of

that period). Rather, this increase is likely due to changes in the large-scale background temperature gradients and potentially land feedbacks. Given the implications of this increase in near-surface warming for future heat waves in Russia, future studies should further examine the robustness of this projection in more models and investigate the underlying mechanism.

In winters, there is a general spatially nonuniform strengthening of all fields, with the exception of temperature anomalies. The stratospheric temperature anomalies in all cases and tropospheric temperature anomalies in some cases, particularly at 850 hPa, are projected to weaken, leading to responses of opposite signs at 850 and 500 hPa in some sectors, for example, over Russia. Furthermore, the response of Z500 is noticeably westward shifted, which is due to the anomalously positive temperature response on the western side of the blocks (even when there is cooling around the center at that level, e.g., over North Pacific). Based on the analysis of the temperature tendency equation performed for reanalysis data, this positive temperature anomaly is attributed to increased upstream latent heating, but this could not be confirmed due to the unavailability of subdaily (or even daily) ω . Based on the LENS dataset alone, in winters, unlike summers, there is substantial weakening of the near-surface warm anomaly under the anticyclone, particularly over North Pacific and Russia.

To summarize, our analysis suggests that latent heating plays an important role in setting the blocking events' 3D structure and its response to climate change, in both seasons and over both land and ocean. These findings add to the growing body of evidence on the importance of latent heating for blocking dynamics that has emerged from a number of recent studies, particularly from pioneering work by Pfahl and collaborators (e.g., Pfahl et al. 2015; Steinfeld and Pfahl 2019; Steinfeld et al. 2020). Our work also shows that to understand the effects of climate change on blocking events and their impact on surface temperature extremes, in particular in summers, further process-level analysis focused on each region, and even with each region separated into at least two clusters, is needed. A thorough analysis requires multimodel, large-ensemble simulation outputs that include subdaily (or at least daily) horizontal and vertical velocity, temperature, and specific humidity, some of which were not available at this point through LENS and GFDL-LE datasets. Such analyses might shed light on the relation between the strength of the blocks and their impact on surface temperature extremes, and the reasons behind the increased near-surface warming in summers and height-dependent response of tropospheric temperature in winters. Additional analysis of changes in synoptic eddy forcings and energetic of blocking events will be needed to investigate the reason(s) for the general strengthening and weakening of most anomalous fields in winters and summers, respectively, and the larger amplitudes of GFDL CM3 responses. That said, the lack of a complete mechanistic understanding of blocking events, and the potential of different mechanisms dominating blocking dynamics in different regions (Drouard and Woollings 2018; Woollings et al. 2018), can complicate answering those questions unambiguously at this point.

Acknowledgments. We are grateful to Gary Lackmann for generously answering our questions about his 2002 paper and we thank the three anonymous reviewers whose comments/suggestions substantially improved the clarity of this manuscript. This work is supported by NSF Grant AGS-1921413 and NASA Grant 80NSSC17K0266. Computational resources were provided by XSEDE (allocation ATM170020), NCAR's CISL (allocation URIC0004), and Rice University Center for Research Computing.

Data availability statement. The ERA-Interim dataset is publicly available from the European Centre for Medium-Range Weather Forecasts (ECMWF) at <https://www.ecmwf.int/en/forecasts/datasets/reanalysis-datasets/era-interim>. Both large-ensemble datasets, the National Center for Atmospheric Research (NCAR) Community Earth System Model (CESM) Large Ensemble Community Project (LENS) and the Geophysical Fluid Dynamics Laboratory (GFDL) Climate Model version 3 (CM3) Large Ensemble Project (GFDL-LE), are publicly available at <http://www.cesm.ucar.edu/projects/community-projects/LENS/> (LENS) and https://www.earthsystemgrid.org/dataset/ucar.cgd.cesm4.CLIVAR_LE.gfdl_cm3_lens.html (GFDL-LE). Both idealized GCMs are available online at <https://mjucker.github.io/MiMA> (moist model) and <https://www.gfdl.noaa.gov/idealized-spectral-models-quickstart/> (dry model).

REFERENCES

- Athanasiadis, P. J., S. Yeager, Y.-O. Kwon, A. Bellucci, D. W. Smith, and S. Tibaldi, 2020: Decadal predictability of North Atlantic blocking and the NAO. *npj Climate Atmos. Sci.*, **3**, 20, <https://doi.org/10.1038/s41612-020-0120-6>.
- Barnes, E. A., and L. M. Polvani, 2015: CMIP5 projections of Arctic amplification, of the North American/North Atlantic circulation, and of their relationship. *J. Climate*, **28**, 5254–5271, <https://doi.org/10.1175/JCLI-D-14-00589.1>.
- , J. Slingo, and T. Woollings, 2012: A methodology for the comparison of blocking climatologies across indices, models and climate scenarios. *Climate Dyn.*, **38**, 2467–2481, <https://doi.org/10.1007/s00382-011-1243-6>.
- , E. Dunn-Sigouin, G. Masato, and T. Woollings, 2014: Exploring recent trends in Northern Hemisphere blocking. *Geophys. Res. Lett.*, **41**, 638–644, <https://doi.org/10.1002/2013GL058745>.
- Barriopedro, D., R. García-Herrera, A. R. Lupo, and E. Hernández, 2006: A climatology of Northern Hemisphere blocking. *J. Climate*, **19**, 1042–1063, <https://doi.org/10.1175/JCLI3678.1>.
- , E. M. Fischer, J. Luterbacher, R. M. Trigo, and R. García-Herrera, 2011: The hot summer of 2010: Redrawing the temperature record map of Europe. *Science*, **332**, 220–224, <https://doi.org/10.1126/science.1201224>.
- Bieli, M., S. Pfahl, and H. Wernli, 2015: A Lagrangian investigation of hot and cold temperature extremes in Europe. *Quart. J. Roy. Meteor. Soc.*, **141**, 98–108, <https://doi.org/10.1002/qj.2339>.
- Brunner, L., and A. K. Steiner, 2017: A global perspective on atmospheric blocking using GPS radio occultation—One decade of observations. *Atmos. Meas. Tech.*, **10**, 4727–4745, <https://doi.org/10.5194/amt-10-4727-2017>.
- , —, B. Scherllin-Pirscher, and M. W. Jury, 2016: Exploring atmospheric blocking with GPS radio occultation

- observations. *Atmos. Chem. Phys.*, **16**, 4593–4604, <https://doi.org/10.5194/acp-16-4593-2016>.
- , G. C. Hegerl, and A. K. Steiner, 2017: Connecting atmospheric blocking to European temperature extremes in spring. *J. Climate*, **30**, 585–594, <https://doi.org/10.1175/JCLI-D-16-0518.1>.
- , N. Schaller, J. Anstey, J. Sillmann, and A. K. Steiner, 2018: Dependence of present and future European temperature extremes on the location of atmospheric blocking. *Geophys. Res. Lett.*, **45**, 6311–6320, <https://doi.org/10.1029/2018GL077837>.
- Cash, B. A., and S. Lee, 2000: Dynamical processes of block evolution. *J. Atmos. Sci.*, **57**, 3202–3218, [https://doi.org/10.1175/1520-0469\(2000\)057<3202:DPOBE>2.0.CO;2](https://doi.org/10.1175/1520-0469(2000)057<3202:DPOBE>2.0.CO;2).
- Cattiaux, J., Y. Peings, D. Saint-Martin, N. Trou-Kechout, and S. J. Vavrus, 2016: Sinuosity of midlatitude atmospheric flow in a warming world. *Geophys. Res. Lett.*, **43**, 8259–8268, <https://doi.org/10.1002/2016GL070309>.
- Chan, P.-W., P. Hassanzadeh, and Z. Kuang, 2019: Evaluating indices of blocking anticyclones in terms of their linear relations with surface hot extremes. *Geophys. Res. Lett.*, **46**, 4904–4912, <https://doi.org/10.1029/2019GL083307>.
- Coumou, D., G. Di Capua, S. Vavrus, L. Wang, and S. Wang, 2018: The influence of Arctic amplification on mid-latitude summer circulation. *Nat. Commun.*, **9**, 2959, <https://doi.org/10.1038/s41467-018-05256-8>.
- Davini, P., and C. Cagnazzo, 2014: On the misinterpretation of the North Atlantic Oscillation in CMIP5 models. *Climate Dyn.*, **43**, 1497–1511, <https://doi.org/10.1007/s00382-013-1970-y>.
- , and F. D'Andrea, 2020: From CMIP3 to CMIP6: Northern Hemisphere atmospheric blocking simulation in present and future climate. *J. Climate*, **33**, 10 021–10 038, <https://doi.org/10.1175/JCLI-D-19-0862.1>.
- Dee, D. P., and Coauthors, 2011: The ERA-Interim reanalysis: Configuration and performance of the data assimilation system. *Quart. J. Roy. Meteor. Soc.*, **137**, 553–597, <https://doi.org/10.1002/qj.828>.
- Dole, R., and N. Gordon, 1983: Persistent anomalies of the extratropical Northern Hemisphere wintertime circulation: Geographical distribution and regional persistence characteristics. *Mon. Wea. Rev.*, **111**, 1567–1586, [https://doi.org/10.1175/1520-0493\(1983\)111<1567:PAOTEN>2.0.CO;2](https://doi.org/10.1175/1520-0493(1983)111<1567:PAOTEN>2.0.CO;2).
- , and Coauthors, 2011: Was there a basis for anticipating the 2010 Russian heat wave? *Geophys. Res. Lett.*, **38**, L06702, <https://doi.org/10.1029/2010GL046582>.
- Donner, L. J., and Coauthors, 2011: The dynamical core, physical parameterizations, and basic simulation characteristics of the atmospheric component AM3 of the GFDL global coupled model CM3. *J. Climate*, **24**, 3484–3519, <https://doi.org/10.1175/2011JCLI3955.1>.
- Drouard, M., and T. Woollings, 2018: Contrasting mechanisms of summer blocking over western Eurasia. *Geophys. Res. Lett.*, **45**, 12–040, <https://doi.org/10.1029/2018GL079894>.
- Dunn-Sigouin, E., and S.-W. Son, 2013: Northern Hemisphere blocking frequency and duration in the CMIP5 models. *J. Geophys. Res. Atmos.*, **118**, 1179–1188, <https://doi.org/10.1002/jgrd.50143>.
- Fischer, E. M., S. I. Seneviratne, P. L. Vidale, D. Lüthi, and C. Schär, 2007: Soil moisture–atmosphere interactions during the 2003 European summer heat wave. *J. Climate*, **20**, 5081–5099, <https://doi.org/10.1175/JCLI4288.1>.
- Galfi, V. M., and V. Lucarini, 2021: Fingerprinting heatwaves and cold spells and assessing their response to climate change using large deviation theory. *Phys. Rev. Lett.*, **127**, 058701, <https://doi.org/10.1103/PhysRevLett.127.058701>.
- Garfinkel, C. I., I. White, E. P. Gerber, M. Jucker, and M. Erez, 2020: The building blocks of Northern Hemisphere wintertime stationary waves. *J. Climate*, **33**, 5611–5633, <https://doi.org/10.1175/JCLI-D-19-0181.1>.
- Green, J., 1977: The weather during July 1976: Some dynamical considerations of the drought. *Weather*, **32**, 120–126, <https://doi.org/10.1002/j.1477-8696.1977.tb04532.x>.
- Hassanzadeh, P., and Z. Kuang, 2015: Blocking variability: Arctic amplification versus Arctic Oscillation. *Geophys. Res. Lett.*, **42**, 8586–8595, <https://doi.org/10.1002/2015GL065923>.
- , and —, 2016: The linear response function of an idealized atmosphere. Part I: Construction using Green's functions and applications. *J. Atmos. Sci.*, **73**, 3423–3439, <https://doi.org/10.1175/JAS-D-15-0338.1>.
- , and —, 2019: Quantifying the annular mode dynamics in an idealized atmosphere. *J. Atmos. Sci.*, **76**, 1107–1124, <https://doi.org/10.1175/JAS-D-18-0268.1>.
- , —, and B. F. Farrell, 2014: Responses of midlatitude blocks and wave amplitude to changes in the meridional temperature gradient in an idealized dry GCM. *Geophys. Res. Lett.*, **41**, 5223–5232, <https://doi.org/10.1002/2014GL060764>.
- , C.-Y. Lee, E. Nabizadeh, S. J. Camargo, D. Ma, and L. Y. Yeung, 2020: Effects of climate change on the movement of future landfalling Texas tropical cyclones. *Nat. Commun.*, **11**, 3319, <https://doi.org/10.1038/s41467-020-17130-7>.
- Hauser, M., R. Orth, and S. I. Seneviratne, 2016: Role of soil moisture versus recent climate change for the 2010 heat wave in western Russia. *Geophys. Res. Lett.*, **43**, 2819–2826, <https://doi.org/10.1002/2016GL068036>.
- Held, I., and M. Suarez, 1994: A proposal for the intercomparison of the dynamical cores of atmospheric general circulation models. *Bull. Amer. Meteor. Soc.*, **75**, 1825–1830, [https://doi.org/10.1175/1520-0477\(1994\)075<1825:APFTIO>2.0.CO;2](https://doi.org/10.1175/1520-0477(1994)075<1825:APFTIO>2.0.CO;2).
- Holmes, C. R., T. Woollings, E. Hawkins, and H. De Vries, 2016: Robust future changes in temperature variability under greenhouse gas forcing and the relationship with thermal advection. *J. Climate*, **29**, 2221–2236, <https://doi.org/10.1175/JCLI-D-14-00735.1>.
- Horton, D. E., N. C. Johnson, D. Singh, D. L. Swain, B. Rajaratnam, and N. S. Diffenbaugh, 2015: Contribution of changes in atmospheric circulation patterns to extreme temperature trends. *Nature*, **522**, 465–469, <https://doi.org/10.1038/nature14550>.
- Hoskins, B. J., and I. N. James, 2014: *Fluid Dynamics of the Mid-Latitude Atmosphere*. John Wiley & Sons, 432 pp.
- , M. E. McIntyre, and A. W. Robertson, 1985: On the use and significance of isentropic potential vorticity maps. *Quart. J. Roy. Meteor. Soc.*, **111**, 877–946, <https://doi.org/10.1002/qj.4971147002>.
- Hsu, P.-C., and T. Li, 2011: Interactions between boreal summer intraseasonal oscillations and synoptic-scale disturbances over the western North Pacific. Part II: Apparent heat and moisture sources and eddy momentum transport. *J. Climate*, **24**, 942–961, <https://doi.org/10.1175/2010JCLI3834.1>.
- Huguenin, M. F., E. M. Fischer, S. Kotlarski, S. C. Scherrer, C. Schwierz, and R. Knutti, 2020: Lack of change in the projected frequency and persistence of atmospheric circulation types over central Europe. *Geophys. Res. Lett.*, **47**, e2019GL086132, <https://doi.org/10.1029/2019GL086132>.
- Hwang, J., P. Martineau, S.-W. Son, T. Miyasaka, and H. Nakamura, 2020: The role of transient eddies in North Pacific blocking formation and its seasonality. *J. Atmos. Sci.*, **77**, 2453–2470, <https://doi.org/10.1175/JAS-D-20-0011.1>.

- Illari, L., and J. C. Marshall, 1983: On the interpretation of eddy fluxes during a blocking episode. *J. Atmos. Sci.*, **40**, 2232–2242, [https://doi.org/10.1175/1520-0469\(1983\)040<2232:OTIOEF>2.0.CO;2](https://doi.org/10.1175/1520-0469(1983)040<2232:OTIOEF>2.0.CO;2).
- Jiang, T., K. Evans, M. Branstetter, P. Caldwell, R. Neale, P. J. Rasch, Q. Tang, and S. Xie, 2019: Northern Hemisphere blocking in 25-km-resolution E3SM v0. 3 atmosphere–land simulations. *J. Geophys. Res. Atmos.*, **124**, 2465–2482, <https://doi.org/10.1029/2018JD028892>.
- Jucker, M., and E. Gerber, 2017: Untangling the annual cycle of the tropical tropopause layer with an idealized moist model. *J. Climate*, **30**, 7339–7358, <https://doi.org/10.1175/JCLI-D-17-0127.1>.
- Kay, J., and Coauthors, 2015: The Community Earth System Model (CESM) large ensemble project: A community resource for studying climate change in the presence of internal climate variability. *Bull. Amer. Meteor. Soc.*, **96**, 1333–1349, <https://doi.org/10.1175/BAMS-D-13-00255.1>.
- Kennedy, D., T. Parker, T. Woollings, B. Harvey, and L. Shaffrey, 2016: The response of high-impact blocking weather systems to climate change. *Geophys. Res. Lett.*, **43**, 7250–7258, <https://doi.org/10.1002/2016GL069725>.
- Kohonen, T., 2012: *Self-Organizing Maps*. Springer, 362 pp.
- Kwon, Y.-O., A. Camacho, C. Martinez, and H. Seo, 2018: North Atlantic winter eddy-driven jet and atmospheric blocking variability in the Community Earth System Model version 1 Large Ensemble simulations. *Climate Dyn.*, **51**, 3275–3289, <https://doi.org/10.1007/s00382-018-4078-6>.
- Lackmann, G. M., 2002: Cold-frontal potential vorticity maxima, the low-level jet, and moisture transport in extratropical cyclones. *Mon. Wea. Rev.*, **130**, 59–74, [https://doi.org/10.1175/1520-0493\(2002\)130<0059:CFPVMT>2.0.CO;2](https://doi.org/10.1175/1520-0493(2002)130<0059:CFPVMT>2.0.CO;2).
- , R. L. Miller, W. A. Robinson, and A. C. Michaelis, 2021: Persistent anomaly changes in high-resolution climate simulations. *J. Climate*, **34**, 5425–5442, <https://doi.org/10.1175/JCLI-D-20-0465.1>.
- Lee, D. Y., and J.-B. Ahn, 2017: Future change in the frequency and intensity of wintertime North Pacific blocking in CMIP5 models. *Int. J. Climatol.*, **37**, 2765–2781, <https://doi.org/10.1002/joc.4878>.
- Lenggenhager, S., M. Croci-Maspoli, S. Brönnimann, and O. Martius, 2019: On the dynamical coupling between atmospheric blocks and heavy precipitation events: A discussion of the southern Alpine flood in October 2000. *Quart. J. Roy. Meteor. Soc.*, **145**, 530–545, <https://doi.org/10.1002/qj.3449>.
- Li, L., R. Zhang, and M. Wen, 2017: Genesis of southwest vortices and its relation to Tibetan Plateau vortices. *Quart. J. Roy. Meteor. Soc.*, **143**, 2556–2566, <https://doi.org/10.1002/qj.3106>.
- Lucarini, V., and A. Gritsun, 2020: A new mathematical framework for atmospheric blocking events. *Climate Dyn.*, **54**, 575–598, <https://doi.org/10.1007/s00382-019-05018-2>.
- Luo, D., W. Zhang, L. Zhong, and A. Dai, 2019: A nonlinear theory of atmospheric blocking: A potential vorticity gradient view. *J. Atmos. Sci.*, **76**, 2399–2427, <https://doi.org/10.1175/JAS-D-18-0324.1>.
- Lupo, A. R., and P. J. Smith, 1995: Planetary and synoptic-scale interactions during the life cycle of a mid-latitude blocking anticyclone over the North Atlantic. *Tellus*, **47A**, 575–596, <https://doi.org/10.3402/tellusa.v47i5.11549>.
- , A. D. Jensen, I. I. Mokhov, A. V. Timazhev, T. Eichler, and B. Efe, 2019: Changes in global blocking character in recent decades. *Atmosphere*, **10**, 92, <https://doi.org/10.3390/atmos10020092>.
- Ma, D., P. Hassanzadeh, and Z. Kuang, 2017: Quantifying the eddy–jet feedback strength of the annular mode in an idealized GCM and reanalysis data. *J. Atmos. Sci.*, **74**, 393–407, <https://doi.org/10.1175/JAS-D-16-0157.1>.
- Ma, J., and X. S. Liang, 2017: Multiscale dynamical processes underlying the wintertime Atlantic blockings. *J. Atmos. Sci.*, **74**, 3815–3831, <https://doi.org/10.1175/JAS-D-16-0295.1>.
- Mak, M., 1991: Dynamics of an atmospheric blocking as deduced from its local energetics. *Quart. J. Roy. Meteor. Soc.*, **117**, 477–493, <https://doi.org/10.1002/qj.49711749904>.
- Masato, G., B. J. Hoskins, and T. Woollings, 2013: Winter and summer Northern Hemisphere blocking in CMIP5 models. *J. Climate*, **26**, 7044–7059, <https://doi.org/10.1175/JCLI-D-12-00466.1>.
- , T. Woollings, and B. Hoskins, 2014: Structure and impact of atmospheric blocking over the Euro-Atlantic region in present-day and future simulations. *Geophys. Res. Lett.*, **41**, 1051–1058, <https://doi.org/10.1002/2013GL058570>.
- Matsueda, M., and H. Endo, 2017: The robustness of future changes in Northern Hemisphere blocking: A large ensemble projection with multiple sea surface temperature patterns. *Geophys. Res. Lett.*, **44**, 5158–5166, <https://doi.org/10.1002/2017GL073336>.
- Nabizadeh, E., P. Hassanzadeh, D. Yang, and E. A. Barnes, 2019: Size of the atmospheric blocking events: Scaling law and response to climate change. *Geophys. Res. Lett.*, **46**, 13 488–13 499, <https://doi.org/10.1029/2019GL084863>.
- Nakamura, H., M. Nakamura, and J. L. Anderson, 1997: The role of high- and low-frequency dynamics in blocking formation. *Mon. Wea. Rev.*, **125**, 2074–2093, [https://doi.org/10.1175/1520-0493\(1997\)125<2074:TROHAL>2.0.CO;2](https://doi.org/10.1175/1520-0493(1997)125<2074:TROHAL>2.0.CO;2).
- Nakamura, N., and C. S. Huang, 2018: Atmospheric blocking as a traffic jam in the jet stream. *Science*, **361**, 42–47, <https://doi.org/10.1126/science.aat0721>.
- Narinesingh, V., J. F. Booth, S. K. Clark, and Y. Ming, 2020: Atmospheric blocking: The impact of topography in an idealized general circulation model. *Wea. Climate Dyn.*, **1**, 293–311, <https://doi.org/10.5194/wcd-2020-2>.
- Patterson, M., T. Bracegirdle, and T. Woollings, 2019: Southern Hemisphere atmospheric blocking in CMIP5 and future changes in the Australia–New Zealand sector. *Geophys. Res. Lett.*, **46**, 9281–9290, <https://doi.org/10.1029/2019GL083264>.
- Peings, Y., J. Cattiaux, S. Vavrus, and G. Magnusdottir, 2017: Late twenty-first-century changes in the midlatitude atmospheric circulation in the CESM large ensemble. *J. Climate*, **30**, 5943–5960, <https://doi.org/10.1175/JCLI-D-16-0340.1>.
- Pfahl, S., and H. Wernli, 2012: Quantifying the relevance of atmospheric blocking for co-located temperature extremes in the Northern Hemisphere on (sub-) daily time scales. *Geophys. Res. Lett.*, **39**, L12807, <https://doi.org/10.1029/2012GL052261>.
- , C. Schwierz, M. Croci-Maspoli, C. M. Grams, and H. Wernli, 2015: Importance of latent heat release in ascending air streams for atmospheric blocking. *Nat. Geosci.*, **8**, 610–614, <https://doi.org/10.1038/ngeo2487>.
- Rasmijn, L., G. van der Schrier, R. Bintanja, J. Barkmeijer, A. Sterl, and W. Hazeleger, 2018: Future equivalent of 2010 Russian heatwave intensified by weakening soil moisture constraints. *Nat. Climate Change*, **8**, 381–385, <https://doi.org/10.1038/s41558-018-0114-0>.
- Rex, D., 1950: Blocking action in the middle troposphere and its effect upon regional climate: I. An aerological study of blocking action. *Tellus*, **2**, 196–211, <https://doi.org/10.3402/tellusa.v2i3.8546>.

- Röthlisberger, M., and O. Martius, 2019: Quantifying the local effect of Northern Hemisphere atmospheric blocks on the persistence of summer hot and dry spells. *Geophys. Res. Lett.*, **46**, 10 101–10 111, <https://doi.org/10.1029/2019GL083745>.
- Schaller, N., J. Sillmann, J. Anstey, E. M. Fischer, C. M. Grams, and S. Russo, 2018: Influence of blocking on northern European and western Russian heatwaves in large climate model ensembles. *Environ. Res. Lett.*, **13**, 054015, <https://doi.org/10.1088/1748-9326/aaba55>. <jrnn>
- Schneider, T., T. Bischoff, and H. Plotka, 2015: Physics of changes in synoptic midlatitude temperature variability. *J. Climate*, **28**, 2312–2331, <https://doi.org/10.1175/JCLI-D-14-00632.1>.
- Schubert, S., and V. Lucarini, 2016: Dynamical analysis of blocking events: Spatial and temporal fluctuations of covariant Lyapunov vectors. *Quart. J. Roy. Meteor. Soc.*, **142**, 2143–2158, <https://doi.org/10.1002/qj.2808>.
- Schwierz, C., M. Croci-Maspoli, and H. Davies, 2004: Perspicacious indicators of atmospheric blocking. *Geophys. Res. Lett.*, **31**, L06125, <https://doi.org/10.1029/2003GL019341>.
- Shutts, G., 1983: The propagation of eddies in diffluent jet-streams: Eddy vorticity forcing of ‘blocking’ flow fields. *Quart. J. Roy. Meteor. Soc.*, **109**, 737–761, <https://doi.org/10.1002/qj.49710946204>.
- Simpson, I. R., and Coauthors, 2020: An evaluation of the large-scale atmospheric circulation and its variability in CESM2 and other CMIP models. *J. Geophys. Res. Atmos.*, **125**, e2020JD032835, <https://doi.org/10.1029/2020JD032835>.
- Small, D., E. Atallah, and J. R. Gyakum, 2013: An objectively determined blocking index and its Northern Hemisphere climatology. *J. Climate*, **27**, 2948–2970, <https://doi.org/10.1175/JCLI-D-13-00374.1>.
- Steinfeld, D., and S. Pfahl, 2019: The role of latent heating in atmospheric blocking dynamics: A global climatology. *Climate Dyn.*, **53**, 6159–6180, <https://doi.org/10.1007/s00382-019-04919-6>.
- , M. Boettcher, R. Forbes, and S. Pfahl, 2020: The sensitivity of atmospheric blocking to changes in upstream latent heating—Numerical experiments. *Wea. Climate Dyn.*, **1**, 405–426, <https://doi.org/10.5194/wcd-1-405-2020>.
- Sun, L., M. Alexander, and C. Deser, 2018: Evolution of the global coupled climate response to Arctic sea ice loss during 1990–2090 and its contribution to climate change. *J. Climate*, **31**, 7823–7843, <https://doi.org/10.1175/JCLI-D-18-0134.1>.
- Thompson, D. W., and Y. Li, 2015: Baroclinic and barotropic annular variability in the Northern Hemisphere. *J. Atmos. Sci.*, **72**, 1117–1136, <https://doi.org/10.1175/JAS-D-14-0104.1>.
- Tsou, C.-H., and P. J. Smith, 1990: The role of synoptic/planetary-scale interactions during the development of a blocking anticyclone. *Tellus*, **42A**, 174–193, <https://doi.org/10.3402/tellusa.v42i1.11869>.
- Ueda, H., H. Kamahori, and N. Yamazaki, 2003: Seasonal contrasting features of heat and moisture budgets between the eastern and western Tibetan Plateau during the GAME IOP. *J. Climate*, **16**, 2309–2324, <https://doi.org/10.1175/2757.1>.
- Wazneh, H., P. Gachon, R. Laprise, A. de Vernal, and B. Tremblay, 2021: Atmospheric blocking events in the North Atlantic: Trends and links to climate anomalies and teleconnections. *Climate Dyn.*, **56**, 2199–2221, <https://doi.org/10.1007/s00382-020-05583-x>.
- Wehrli, K., B. P. Guillod, M. Hauser, M. Leclair, and S. I. Seneviratne, 2019: Identifying key driving processes of major recent heat waves. *J. Geophys. Res. Atmos.*, **124**, 11 746–11 765, <https://doi.org/10.1029/2019JD030635>.
- Wiedenmann, J. M., A. R. Lupo, I. I. Mokhov, and E. A. Tikhonova, 2002: The climatology of blocking anticyclones for the Northern and Southern Hemispheres: Block intensity as a diagnostic. *J. Climate*, **15**, 3459–3473, [https://doi.org/10.1175/1520-0442\(2002\)015<3459:TCOBAF>2.0.CO;2](https://doi.org/10.1175/1520-0442(2002)015<3459:TCOBAF>2.0.CO;2).
- Woollings, T., and Coauthors, 2018: Blocking and its response to climate change. *Curr. Climate Change Rep.*, **4**, 287–300, <https://doi.org/10.1007/s40641-018-0108-z>.
- Yamazaki, A., and H. Itoh, 2013: Vortex–vortex interactions for the maintenance of blocking. Part I: The selective absorption mechanism and a case study. *J. Atmos. Sci.*, **70**, 725–742, <https://doi.org/10.1175/JAS-D-11-0295.1>.
- Yanai, M., and T. Tomita, 1998: Seasonal and interannual variability of atmospheric heat sources and moisture sinks as determined from NCEP–NCAR reanalysis. *J. Climate*, **11**, 463–482, [https://doi.org/10.1175/1520-0442\(1998\)011<0463:SAIVOA>2.0.CO;2](https://doi.org/10.1175/1520-0442(1998)011<0463:SAIVOA>2.0.CO;2).
- , S. Esbensen, and J.-H. Chu, 1973: Determination of bulk properties of tropical cloud clusters from large-scale heat and moisture budgets. *J. Atmos. Sci.*, **30**, 611–627, [https://doi.org/10.1175/1520-0469\(1973\)030<0611:DOBPOT>2.0.CO;2](https://doi.org/10.1175/1520-0469(1973)030<0611:DOBPOT>2.0.CO;2).
- Zschenderlein, P., A. H. Fink, S. Pfahl, and H. Wernli, 2019: Processes determining heat waves across different European climates. *Quart. J. Roy. Meteor. Soc.*, **145**, 2973–2989, <https://doi.org/10.1002/qj.3599>.
- , S. Pfahl, H. Wernli, and A. H. Fink, 2020: A Lagrangian analysis of upper-tropospheric anticyclones associated with heat waves in Europe. *Wea. Climate Dyn.*, **1**, 191–206, <https://doi.org/10.5194/wcd-1-191-2020>.

Copyright of Journal of Climate is the property of American Meteorological Society and its content may not be copied or emailed to multiple sites or posted to a listserv without the copyright holder's express written permission. However, users may print, download, or email articles for individual use.